ADVANCING EARTH AND SPACE SCIENCES

JGR Atmospheres

RESEARCH ARTICLE
10.1029/2026JD047324

Features of Regional Compound Dry-Hot Events Over the Yangtze River Basin in Warm Season and Related Mechanisms

Yunfei Cai[1], Anning Huang[1,2], Yaocun Zhang[1], Lijuan Wen[3], Rongchang Wu[1], Shanshan Li[1], Jingwen Zeng[1], Ziqi Li[1], and Yaqing Sha[1]

[1]School of Atmospheric Sciences, Nanjing University, Nanjing, China, [2]Qinghai Lake Comprehensive Observation Research Station, Chinese Academy of Sciences, Gangcha, China, [3]Key Laboratory of Land Surface Process and Climate Change in Cold and Arid Regions, Chinese Academy of Sciences, Lanzhou, China

Key Points:

- Two synoptic patterns drive the occurrence of regional compound dry-hot events (RCDHEs) in the Yangtze River Basin (YRB) in warm season
- The intensity and occurrence of RCDHEs show significant increasing trends during 1961–2024 and increase at a much faster rate after 2000
- The decreased cloud cover and precipitation and enhanced surface heating in the YRB due to an abnormal high pressure sustain the RCDHEs

Correspondence to:

A. Huang,
anhuang@nju.edu.cn

Citation:

Cai, Y., Huang, A., Zhang, Y., Wen, L., Wu, R., Li, S., et al. (2026). Features of regional compound dry-hot events over the Yangtze River Basin in warm season and related mechanisms. *Journal of Geophysical Research: Atmospheres*, *131*, e2026JD047324. https://doi.org/10.1029/2026JD047324

Received 25 APR 2026
Accepted 28 AUG 2026

Author Contributions:
Conceptualization: Anning Huang
Data curation: Yunfei Cai, Anning Huang
Formal analysis: Yunfei Cai, Anning Huang, Yaocun Zhang, Lijuan Wen, Rongchang Wu, Shanshan Li, Jingwen Zeng, Ziqi Li, Yaqing Sha
Investigation: Yunfei Cai, Anning Huang, Yaocun Zhang, Lijuan Wen, Rongchang Wu, Shanshan Li, Jingwen Zeng, Ziqi Li, Yaqing Sha
Methodology: Yunfei Cai, Anning Huang
Resources: Yunfei Cai, Anning Huang, Yaocun Zhang, Lijuan Wen, Shanshan Li
Software: Yunfei Cai
Supervision: Anning Huang
Validation: Yunfei Cai, Anning Huang, Yaocun Zhang, Lijuan Wen, Rongchang Wu
Visualization: Yunfei Cai
Writing – original draft: Yunfei Cai, Anning Huang

Abstract Based on daily station observations and ERA5 reanalysis data during warm seasons of 1961–2024, the characteristics of regional compound dry-hot events (RCDHEs) and associated mechanisms over Yangtze River Basin (YRB) have been systematically explored. Results show more than 45% of the total occurrence days (OD) of compound dry-hot events (CDHEs) over most YRB in warm season is contributed by the RCDHEs, which show distinct sub-seasonal variations and concentrate in mid-June to mid-July. The coverage rate (CR), intensity and OD of RCDHEs all show significant increasing trends during 1961–2024, especially as the intensity and OD increase at much faster rates after 2000. Moreover, the occurrences of RCDHEs are mainly driven by two synoptic patterns named P1 and P2, respectively. The P1 (P2) pattern features that the intensified Western Pacific Subtropical High and South Asian High with southerly (northerly) location relative to the climatology move toward each other. Meanwhile, the intensity, CR and OD of RCDHEs under both P1 and P2 patterns all show increasing trends during 1961–2024, and the accelerated increasing rates of the intensity and OD after 2000 are mainly contributed by those under the P1 pattern. Mechanism analysis reveals that the decreased cloud cover and precipitation in southern (central-eastern) YRB due to the subsidence induced by the abnormal high pressure under the P1 (P2) pattern enhance the surface net shortwave radiation and heating there, further leading to much higher occurrence probability of CDHEs in southern (central-eastern) YRB during the RCDHEs under the P1 (P2) pattern.

Plain Language Summary As one of the most densely populated and agriculturally important regions in the world, the Yangtze River Basin (YRB) is severely suffered by regional compound dry-hot events (RCDHEs) characterized by their large spatial extent and long duration. This study revealed that RCDHEs lead to more than 45% of the total occurrence days (OD) of station-scale compound dry-hot events in most YRB. Both the OD and intensity of RCDHEs experienced clear increasing trends during past 60 years with the increasing rates accelerated after 2000. Meanwhile, these RCDHEs are often closely associated with two typical synoptic circulation patterns that create persistent dry and unusually hot conditions over the YRB. Under these synoptic patterns, decreases of cloud cover and rainfall lead to more sunlight reaches the land surface which causes the ground to heat more strongly and increases the likelihood of hot and dry compound extremes. These findings help explain why the RCDHEs in the YRB are becoming much more severe and provide scientific support for improving climate risk assessment disaster preparedness and adaptation planning in vulnerable regions.

1. Introduction

Under global warming the frequency of spatiotemporal coupling between extreme heat and drought has increased significantly (Seneviratne et al., 2021; Sippel et al., 2020). Compound dry-hot events (CDHEs) are formed through this coupling and produce nonlinear amplification effects via physical processes such as soil-atmosphere feedback (Fischer et al., 2007; Miralles et al., 2019). Their impacts far exceed those of the individual extreme events (Leonard et al., 2014; Zscheischler et al., 2018). The CDHEs over the Europe and the Yangtze River Basin (YRB), China in 2022 caused tens of thousands of deaths and severe agricultural losses and energy crises (Y. Liu, Yuan, et al., 2023; Toreti et al., 2022). These events have highlighted the urgent need to understand the formation mechanisms of CDHEs (AghaKouchak et al., 2020; Ridder et al., 2020). Regional compound dry-hot events (RCDHEs), characterized by their large spatial extent and long duration, pose more severe systemic risks to

10.1029/2026JD047324

Writing – review & editing: Anning Huang, Yaocun Zhang, Lijuan Wen, Rongchang Wu, Shanshan Li, Jingwen Zeng, Ziqi Li, Yaqing Sha

socioeconomic systems by simultaneously affecting multiple critical sectors such as agriculture, water resources, and energy (Mukherjee & Mishra, 2021; Raymond et al., 2020). Unlike local CDHEs, the spatially coherent structure of RCDHEs reflects dominant synoptic-scale forcing, making them more amenable to dynamic diagnosis and prediction. Understanding of RCDHEs in depth is therefore directly related to the effectiveness of regional adaptation strategies (Vogel et al., 2017; H. Wu et al., 2023).

RCDHEs are regional responses to large-scale circulation anomalies and their spatially coherent structures can effectively capture the dominant signals of synoptic systems such as persistent blocking highs and subtropical high anomalies (Kornhuber et al., 2020; Pfahl & Wernli, 2012). This provides a critical pathway for diagnosing the dynamic linkages between circulation patterns and extreme events (Teng & Branstator, 2019; P. Xu et al., 2020). However existing studies mostly adopt monthly-scale climate data to identify the spatiotemporal overlap between droughts and heat waves (Alizadeh et al., 2020; Weynants et al., 2025). The temporal resolution mismatch between monthly-scale standardized precipitation index (SPI) and daily-scale heat wave indices leads to systematic biases. Flash droughts lasting 3–4 weeks may be fragmented or missed if they cross monthly boundaries (Ford & Labosier, 2017; Pendergrass et al., 2020). Monthly aggregation cannot capture the synoptic-scale co-evolution and positive feedback processes between droughts and heat waves (Manning et al., 2018; Schumacher et al., 2019), constraining identification of predictability signals (Domeisen et al., 2022; Vitart & Robertson, 2018). Therefore, establishing daily-scale identification methods for RCDHEs is crucial for characterizing their spatiotemporal evolution and revealing coupling mechanisms with synoptic-scale circulation anomalies (H. Chen & Sun, 2015; X. Zhang et al., 2023).

The YRB is located in the core of East Asian monsoon-influenced region where the warm season climate is influenced by the Western Pacific Subtropical High (WPSH), the South Asian High (SAH) and the East Asian subtropical jet (EASJ) (B. Wang et al., 2021; Yihui & Chan, 2005). Anomalously westward and intensified WPSH causes persistent radiative warming and precipitation deficits amplified by soil-atmosphere feedbacks (Luo & Lau, 2018; Miralles et al., 2019), making the YRB a hotspot of RCDHEs in recent years (D. Chen et al., 2024; Kong et al., 2020; Sun et al., 2014). While existing studies emphasize the WPSH dominance in the occurrences of RCDHEs (Y. Ding et al., 2007; Lee et al., 2023), recent evidence suggests multiple circulation systems including SAH and mid-latitude blocking play critical roles (Singh et al., 2022; Yuan et al., 2019). The East Asian summer monsoon experienced significant interdecadal transition around the late 1990s to early 2000s (Y. Ding et al., 2008; Si & Ding, 2016), potentially altering the circulation configurations for RCDHEs (R. Ding et al., 2010; Yim et al., 2014). Furthermore, the systematic identification of RCDHEs and their circulation patterns across interdecadal periods remains insufficient (Bevacqua et al., 2023; X. Wu et al., 2021), highlighting the need for objective weather pattern classification (Feng et al., 2025; Jouan et al., 2023; W. Xu et al., 2024).

Recent studies have substantially advanced the understanding of RCDHEs over the YRB, particularly following the unprecedented RCDHE of summer 2022, which caused severe impacts on agriculture, water resources, and energy systems (Feng et al., 2024; Yin et al., 2025; Y. Zhang et al., 2026). Anthropogenic warming has been identified as an important factor increasing the likelihood and intensity of such extreme events (D. Chen et al., 2024). Land-atmosphere interactions and soil moisture feedbacks have also been shown to substantially amplify the persistence and intensity of the 2022 event (X. Chen et al., 2025). Recent studies further emphasized that vegetation-land-atmosphere interactions can reinforce cascading drought-heat extremes under favorable hydroclimatic conditions (An et al., 2025). Future projections also suggest that RCDHEs will become more frequent and intense under continued climate warming (Y. Zhang et al., 2026). However, existing studies have mainly focused on individual extreme events, future projections, or monthly-scale statistics. The long-term evolution of daily RCDHEs and their dominant synoptic circulation patterns therefore remain poorly understood.

Objective weather pattern identification is critical for understanding compound extreme events (Huth et al., 2008; Tuel & Martius, 2021). Traditional single-level clustering methods based on geopotential height fields cannot capture the coordinated multi-level circulation anomalies involving the upper-level anticyclones and low-level moisture deficits (Ayarzagüena et al., 2018; Philipp et al., 2010). Machine learning approaches have emerged as powerful tools to identify such complex nonlinear atmospheric patterns (Mamalakis et al., 2022; Toms et al., 2020). Spectral clustering can objectively detect arbitrarily shaped circulation regimes in high-dimensional atmospheric data sets without predefined assumptions (Albers & Newman, 2021; von Luxburg, 2007). This technique demonstrates higher skill than conventional methods in classifying synoptic patterns associated with precipitation extremes (Gibson et al., 2021; Salcedo-Sanz et al., 2024).

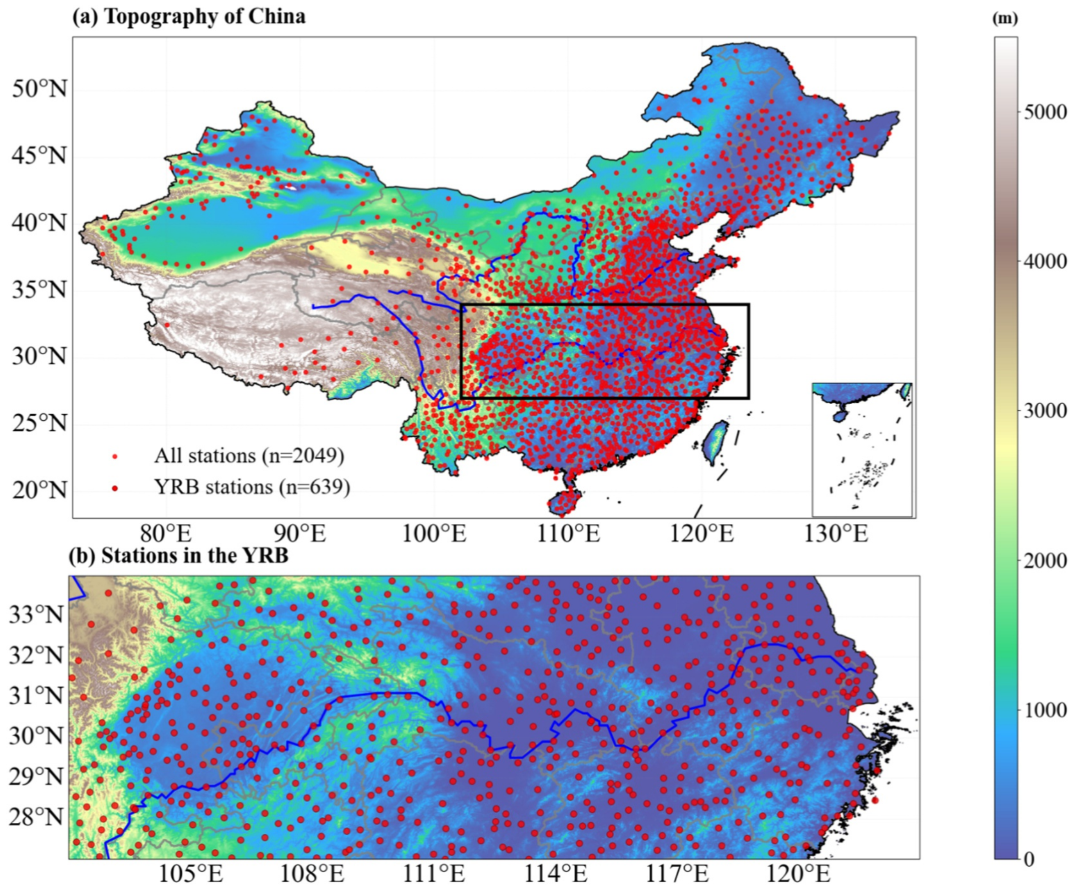

Figure 1. (a) Distribution of topography (shadings) and meteorological stations (red dot) in China with the location of the Yangtze River Basin (YRB) (black box). (b) Topography (shadings) and 639 meteorological stations (red dots) in YRB. Blue line shows the Yangtze River.

To address the limitations of previous single-event studies and monthly-scale climate statistics (Bevacqua et al., 2023; Ridder et al., 2020), this study develops a daily-scale method to identify and characterize warm-season RCDHEs, objectively classifies their dominant synoptic circulation patterns using spectral clustering (R. Wu et al., 2025; Zhou et al., 2025), and quantifies the contributions of different circulation patterns to the long-term evolution of RCDHEs over the YRB. Specifically, this study aims to answer the following questions: What are the key characteristics and interdecadal changes of warm-season RCDHEs over the YRB, and what are their dominant synoptic patterns? What are the physical mechanisms which induce warm-season RCDHEs over the YRB under different synoptic patterns?

2. Data and Methods

2.1. Data

The data used in this study are listed as follows:

1. The daily precipitation data and maximum temperature data observed at 2049 meteorological stations which are distributed across China (Figure 1a), and 639 stations in the YRB (Figure 1b) during the warm seasons (May to October) of 1961–2024, which are qualified and provided by the China Meteorological Administration (CMA; available at http://data.cma.cn). In this study, the YRB refers to the region spanning 102°–122°E, 27°–34°N, where 639 meteorological stations with reliable long-term observations are distributed.
2. The hourly ERA5 reanalysis data set with the spatial resolution of 0.25° during the warm seasons (May–October) of 1961–2024, including the *u*- and *v*-components of wind, geopotential height, specific humidity, vertical velocity and cloud cover at 37 pressure levels, and surface sensible heat flux (positive upward), latent

heat flux (positive upward), net shortwave radiation (positive downward), and net longwave radiation (positive downward), which are provided by the European Centre for Medium-Range Weather Forecasts (Hersbach et al., 2020).

2.2. Definition of RCDHEs

Step 1: Detection of station-level CDHEs

The hot events are identified using a relative threshold method (Fu & Wang, 2023). For the station i on the calendar day j of the year k, a 15-day moving window centered on the calendar day j is constructed, including the 7 days before and after the target day. Daily maximum temperatures within this window from all warm seasons of 1961–2024 are extracted, yielding a reference sample of 15×64 values for each calendar day at each station. The 90th percentile of this sample is defined as the extreme high-temperature threshold denoted by $T90_{i,j}$ (Russo et al., 2015). If the daily maximum temperature $T_{i,j,k}$ at the station i on the calendar day j of the year k exceeds the corresponding threshold $T90_{i,j}$, the calendar day j of the year k is identified as a hot day for the station i.

The dry days are identified using the 30-day Standardized Precipitation Index (SPI30), which characterizes short-term meteorological drought conditions (Bjerre et al., 2026; Xiong et al., 2025). Because the daily precipitation exhibits strong random fluctuations, the SPI is not calculated at the single-day scale. Instead, a 30-day rolling cumulative precipitation is first computed for each station:

$$R30_{i,j,k} = \sum_{m=j-29}^{j} P_{i,j,k} \tag{1}$$

where $P_{i,j,k}$ is the daily precipitation (units: mm) at the station i on the calendar day m of the year k, and $R30_{i,j,k}$ is the cumulative precipitation of the preceding 29 days and the calendar day j of the year k at the station i. For the station i on the calendar day j, all historical $R30_{i,j,k}$ within the 15-day moving window centered on the calendar day j during the period of 1961–2024 are extracted to form a reference sample, giving $15 \times 64 = 960$ samples for each calendar day. Since some $R30_{i,j,k}$ values are zero, a mixed distribution with zero-value correction is adopted. The probability of zero precipitation is estimated by

$$P0_{i,j,k} = \frac{N0_{i,j,k}}{N} \tag{2}$$

where $N0_{i,j,k}$ is the number of samples with $R30_{i,j,k} = 0$ in the reference samples of $N = 960$ for the station i and calendar day j of the year k.

The cumulative probability of $R30_{i,j,k}$ is then calculated by

$$H_{i,j,k}(R30_{i,j,k}) = \begin{cases} P0_{i,j,k} & R30_{i,j,k} = 0 \\ P0_{i,j,k} + (1 - P0_{i,j,k}) \cdot f(R30_{i,j,k}; \alpha_{i,j,k}, \beta_{i,j,k}) & R30_{i,j,k} > 0 \end{cases} \tag{3}$$

For positive precipitation accumulations ($R30_{i,j,k} > 0$), a two-parameter Gamma distribution function which is fitted using maximum likelihood estimation is given by:

$$f(x; \beta, \theta) = \frac{x^{\beta-1} e^{-x/\theta}}{\Gamma(\beta)\theta^{\beta}} \qquad x > 0 \tag{4}$$

where $f(x; \beta, \theta)$ is the cumulative distribution function of the fitted Gamma distribution. According to the approximation proposed (Thom, 1958), the shape parameter $\beta = \frac{\bar{x}^2}{s^2}$ and scale parameter $\theta = \frac{1}{\beta}$, $\bar{x}$ (s^2) is the mean (variance) of positive x in a time series with sample N, which is 960 in this study. And $\Gamma(\beta) = \int_0^{\infty} t^{\beta-1} e^{-t} dt$ is the Gamma function.

Finally, the cumulative probability is transformed to the standard normal space to obtain SPI30:

$$\mathrm{SPI30}_{i,j,k} = \varphi^{-1}\left[H_{i,j,k}\left(R30_{i,j,k}\right)\right] \tag{5}$$

where $\varphi^{-1}(z) = \int_{-\infty}^{z} \frac{1}{\sqrt{2\pi}} e^{\frac{-t^2}{2}} dt$ is the quantile function of the standard normal distribution (Sutanto et al., 2024). Following the classification criteria established in previous studies (McKee et al., 1993), to quantify the intensity of such compound dry-hot conditions, the compound dry-hot magnitude index (CDHMI) for station i on the calendar day j of the year k is calculated by

$$\mathrm{CDHMI}_{i,j,k} = \begin{cases} \left(\left|\mathrm{SPI30}_{i,j,k}\right| - 0.5\right) \times \left(\dfrac{T_{i,j,k} - T90_{i,j}}{\sigma_{i,j}}\right), & \text{if } \mathrm{SPI30}_{i,j,k} < -0.5 \text{ and } T_{i,j,k} \geq T90_{i,j} \\ 0, & \text{otherwise} \end{cases} \tag{6}$$

$T_{i,j,k}$ is the daily maximum temperature at the station i on the calendar day j of the year k; and $\sigma_{i,j}$ is the standard deviation of daily maximum temperature for the station i at the calendar day j, it is calculated by

$$\sigma_{i,j} = \sqrt{\frac{1}{iy} \sum_{k=1}^{iy} \left(T_{i,j,k} - \overline{T}_{i,j}\right)^2} \tag{7}$$

$\overline{T}_{i,j} = \frac{1}{iy} \sum_{k=1}^{iy} T_{i,j,k}$ is the multi-year mean daily maximum temperature at the station i on the calendar day j, and $iy = 64$ is the total number of years during the period of 1961–2024. A station-level CDHE is identified if $\mathrm{CDHMI}_{i,j,k} > 0$ (Zscheischler et al., 2018). The CDHEs identified here are concurrent compound events (Zscheischler et al., 2020), in which drought ($\mathrm{SPI30}_{i,j,k} < -0.5$) and extreme heat ($T_{i,j,k} \geq T90_{i,j}$) conditions are simultaneously satisfied on the same day. Sequential CDHEs are not considered in this study. The robustness of the identified RCDHEs to the choice of the SPI accumulation period (SPI15, SPI30, SPI45), the spatial coverage thresholds (initiation/continuation: 15%/5%, 20%/8%, 25%/10%), and the maximum interruption duration (3, 5, 7 days) has been examined through sensitivity analyses, which confirm that the main conclusions of this study are insensitive to these methodological choices.

Step 2: Detection of RCDHEs in the YRB

Based on daily observations from 639 stations within the YRB, RCDHEs are identified according to the number of stations simultaneously experiencing station-level CDHEs during the warm seasons of 1961–2024. The $M_{j,k}$ denote the number of stations simultaneously with $\mathrm{CDHMI}_{i,j,k} > 0$ on the day j of the year k. The first day with the number of stations with $M_{j,k} \geq 127$ (i.e., regional coverage ≥ 20%) is taken as the start day of a RCDHE (Guo et al., 2017; R. Wu et al., 2025). After the event starts, the following days are treated as part of the same event if $M_{j,k} \geq 51$ (coverage ≥ 8%) (Sheffield et al., 2009). If $M_{j,k} < 51$ (coverage < 8%) for no more than 5 consecutive days, and $M_{j,k}$ later returns to $M_{j,k} \geq 51$, the interrupted period is still considered as part of the same RCDHE (McKee et al., 1993; Russo et al., 2014). If the consecutive below-threshold ($M_{j,k} < 51$) period exceeds 5 days, the event is considered to end on the last day with $M_{j,k} \geq 51$ before the interruption. According to the method mentioned above, 94 RCDHEs with 868 days are identified and they are generally consistent with the major historical RCDHEs reported in previous studies (D. Chen et al., 2024; T. Ding et al., 2010; Li et al., 2011; L. Zhang & Zhou, 2015). Detailed identification processes for a representative event in 2006 are shown in Figure 2.

2.3. Clustering Analysis of the Dominant Synoptic Pattern for the RCDHEs

The spectral clustering method based on graph theory first constructs a similarity matrix and Laplacian matrix from the input data and then obtains the corresponding eigenvectors and clusters (Donath & Hoffman, 1973; J. Liu & Han, 2018). It has been used to identify the dominant synoptic patterns of extreme weather and climate events (Y. Tang et al., 2021; R. Wu et al., 2025; X. Xu et al., 2023). The four pressure levels (850, 700, 500, and 200 hPa)

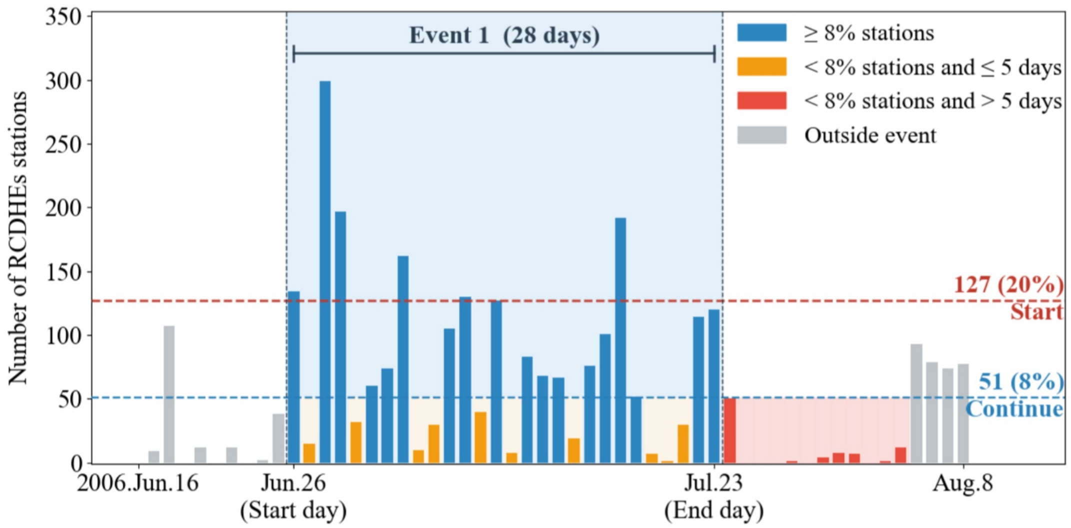

Figure 2. Illustration of regional compound dry-hot event (RCDHE) identification using a representative event in 2006. Bars show the daily number of stations with simultaneous CDHE occurrence. The light blue shaded background indicates the duration of the identified RCDHE. The red dashed line marks the start threshold (127 stations, 20% of all stations in the Yangtze River Basin (YRB)), and the blue dashed line marks the continuation threshold (51 stations, 8%). Bar colors indicate different day categories within and outside the identified RCDHE: blue bars denote days when the number of stations with simultaneous CDHE occurrence is ≥8% of total YRB stations (continuation criterion met); orange bars denote days below the 8% threshold but lasting no more than five consecutive days (allowable interruption period, still considered part of the event); red bars denote days below the 8% threshold lasting more than five consecutive days (event termination criterion reached); and gray bars denote days outside the identified RCDHE.

were selected to represent the low-level moisture transport, mid-tropospheric convergence, WPSH, and SAH, respectively, thereby capturing the full vertical structure of the tropospheric circulation associated with RCDHEs. Wind fields rather than geopotential height were adopted as input because they provide a more complete kinematic description of the atmospheric circulation, including non-geostrophic components and vertical wind shear critical for characterizing upper–lower tropospheric coupling (Niu et al., 2026; Zeng et al., 2025). To explore the atmospheric circulation characteristics during the RCDHEs, the ERA5 u and v wind components at four pressure levels (200, 500, 700, and 850 hPa) over the YRB region (102°–122°E, 27°–34°N) at all occurrence days (OD) of RCDHEs (a total of 868 days) are used as input data for spectral clustering. The spatial dimensions of wind speed components for each RCDHE day (height: 4, latitude: 29, longitude: 81) are first reshaped into a one-dimensional array ($4 \times 29 \times 81 = 9{,}396$). Then the v component array is concatenated after the u component array to form a complete spatial array ($9{,}396 \times 2 = 18{,}792$). Next, for the 868-day samples of RCDHEs, a two-dimensional array (number of samples: 868, number of features: 18,792) is constructed and standardized along the sample dimensions as input data for spectral clustering (Prodregosa, 2011). The main purpose of standardization is to scale the value ranges of wind fields at different pressure levels to the same scale, avoiding disproportionate influence of certain features on the results due to differences in value ranges during the clustering process. Finally, the highest Calinski-Harabasz score is used to determine the number of clusters for spectral clustering (Caliński & Harabasz, 1974). In summary, the multi-level wind field configuration is used as circulation features for the RCDHEs to obtain clustering results that reflect the synergistic configurations of circulations at upper and lower troposphere.

2.4. Metrics for the RCDHEs and Their Associated Synoptic Patterns

Some attributes are defined to characterize each RCDHE in Equations 9–12. For the mth RCDHE ($m = 1, 2, \ldots, M$), the total number of RCDHEs is 94, so $M = 94$. The ts_m and te_m denote the start day and end day of the mth RCDHE, respectively. $N_{t,m}$ represents the total number of stations simultaneously experiencing CDHE on the day t during the mth RCDHE, and $r_{s,m,t}$ denotes the CDHMI > 0 at the station s ($s = 1, 2, \ldots, N_{t,m}$) on the day t during the mth RCDHE.

The mean intensity of each RCDHE is calculated according to Equation 8. The duration of each RCDHE is calculated by Equation 9. The coverage rate (CR) in Equation 10 represents the average for the ratio of the area affected by each RCDHE to the total area of YRB. The regional mean intensity of each RCDHE in Equation 11 indicates the total accumulated $r_{\mathrm{i,t,m}}$ distributed evenly across the total stations (639) of the YRB. Notably, Equation 11 can be directly written as the product of Equations 8–10, that is, regional mean intensity $_m$ = Intensity$_m$ × Duration$_m$ × Coverage rate$_m$. To characterize the interannual variability, let M_k denote the total number of RCDHEs occurring in the year k, where $\sum_{k=1}^{64} M_k = 94$ is the total number of RCDHEs during the period of 1961–2024 (total 64 years). The annual OD of RCDHEs is the total cumulative duration of all RCDHEs in each year ($\sum_{l=1}^{M_k}$ Duration$_l$), while the annual mean intensity, CR, and regional mean intensity are computed as the arithmetic mean of the corresponding RCDHE across the M_k events in each year. For instance, if $M_k = 2$ with duration of 5 and 8 days and regional mean intensity of 0.3 and 0.5, respectively, the annual OD is 13 days and the annual mean regional mean intensity is 0.4. These four quantities of each RCDHE are defined as follows:

$$\text{Intensity}_m = \frac{\sum_{t=ts_m}^{t=te_m} \sum_{s=1}^{N_{t,m}} r_{s,t,m}}{\sum_{t=ts_m}^{t=te_m} N_{t,m}} \tag{8}$$

$$\text{Duration}_m = (te_m - ts_m + 1) \tag{9}$$

$$\text{Coverage rate}_m = \frac{\sum_{t=ts_m}^{t=te_m} N_{t,m}}{639 \times (te_m - ts_m + 1)} \tag{10}$$

$$\text{regional mean intensity}_m = \frac{\sum_{ts_m}^{te_m} \sum_{s=1}^{N_{t,m}} r_{s,t,m}}{639} \tag{11}$$

The occurrence probability (OP) of CDHEs at each station is defined as the ratio of O_i (the total number of days that the station i experienced CDHE during all RCDHEs) to $\sum_{m=1}^{M}$ Duration$_m$ (the total OD of all RCDHEs) is expressed by:

$$\text{Occurrence probability}_i = \frac{O_i}{\sum_{m=1}^{M} \text{Duration}_m} \times 100\% \tag{12}$$

To quantitatively diagnose the mechanisms maintaining temperature anomalies under different synoptic patterns, the thermodynamic equation in pressure coordinates is used to evaluate the contribution of each term to the temperature tendency. The temperature tendency (dt) can be decomposed into horizontal advection terms (x_adv and y_adv), vertical motion term (z_mot), and diabatic heating term (DHT) (W. Liu et al., 2024; Zeng et al., 2025). The equation is defined as follows:

$$\underbrace{\frac{\partial T}{\partial t}}_{dt} = \underbrace{-u\frac{\partial T}{\partial x}}_{x\_\text{adv}} \underbrace{-v\frac{\partial T}{\partial y}}_{y\_\text{adv}} \underbrace{-\omega\frac{\partial T}{\partial p} + \frac{R}{C_p p}T\omega}_{z\_\text{mot}} + \text{DHT} \tag{13}$$

where T is air temperature; u and v are the zonal and meridional wind components, respectively; ω is the vertical velocity in pressure coordinates (Pa s^{-1}); $R = 287$ J kg^{-1}K^{-1} is the gas constant for dry air; $C_p = 1{,}004$ J kg^{-1}K^{-1} is the specific heat at constant pressure; p is pressure; and dt is the temperature tendency. The term $-u\frac{\partial T}{\partial x}$ (x_adv) represents the zonal temperature advection, $-v\frac{\partial T}{\partial y}$ (y_adv) represents the meridional temperature advection, $-\omega\frac{\partial T}{\partial p} + \frac{R}{C_p p}T\omega$ (z_mot) represents the vertical motion term, and DHT represents the diabatic heating term, which likely reflects the combined effect of net radiative heating, latent heat release, and other unresolved diabatic processes. The thermodynamic budget is estimated at near surface, and all terms are composited during RCDHEs under each synoptic pattern.

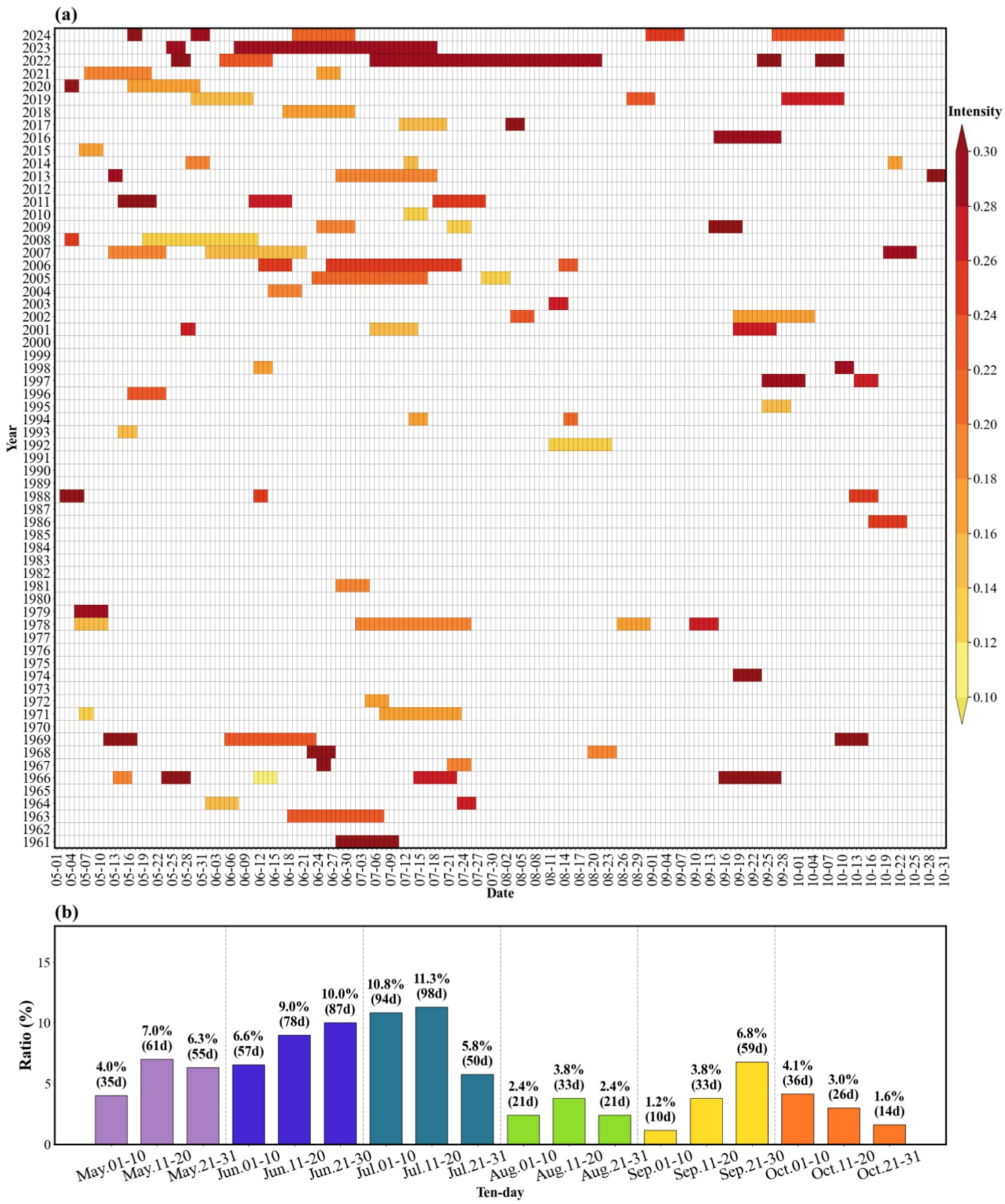

Figure 3. (a) Year-by-year distribution of warm-season regional compound dry-hot events (RCDHEs) in the Yangtze River Basin during the period of 1961–2024. Each horizontal bar represents one RCDHE, with bar length indicating duration (days) and color indicating the intensity. (b) Ratios of the total RCDHE occurrence days (OD) within each 10-day of May–October in 1961–2024 to the total RCDHE OD in the warm seasons of 1961–2024. The total RCDHE OD within each 10-day of May–October in 1961–2024 are shown in parentheses of panel (b).

In addition, this study also defined several synoptic circulation systems, including the SAH at 200 hPa with a threshold of 12,500 gpm, the WPSH at 500 hPa with a threshold of 5,880 gpm, and the EASJ at 200 hPa, represented by the axis of the upper-tropospheric westerly jet over East Asia (Ge et al., 2019; Y. Liu, Huang, et al., 2023; Ning et al., 2017). The abrupt interdecadal shift in annual OD of RCDHE is detected using a 10-year moving t-test (Sassi et al., 2009). The significance of linear trends is assessed using the Mann-Kendall test (Yue & Wang, 2004).

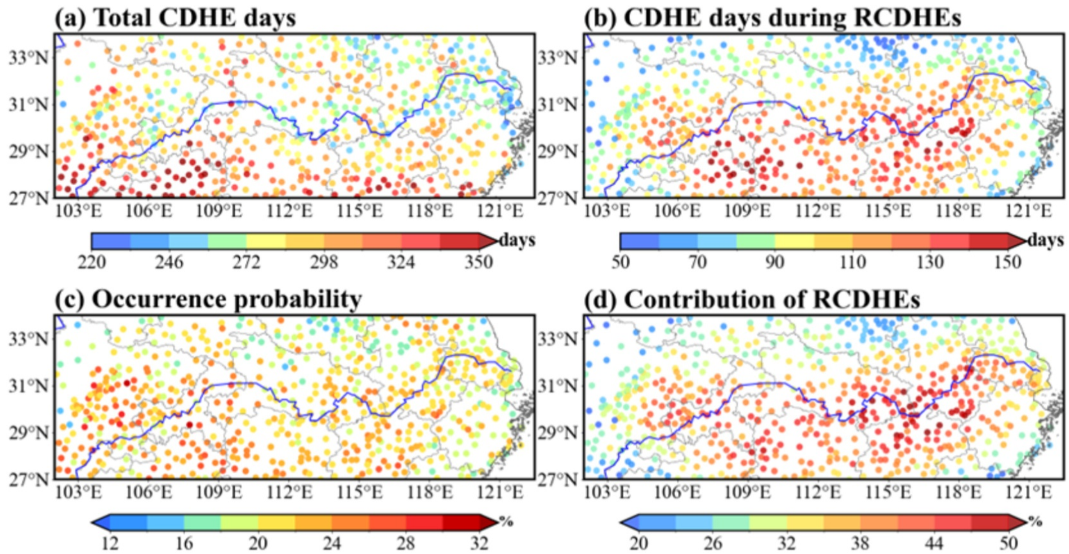

Figure 4. (a) The total occurrence days (OD) of compound dry-hot events (CDHEs) at each station during the warm seasons of 1961–2024. (b) The total OD of CDHEs at each station during the regional compound dry-hot events (RCDHEs) in the warm seasons of 1961–2024. (c) The occurrence probability of CDHEs at each station during RCDHEs. (d) Contribution of RCDHEs to the total CDHEs at each station, which is defined as the ratio of (b) to (a). The blue line indicates the Yangtze River.

3. Results

3.1. Characteristics of Warm-Season RCDHEs Over the YRB

As shown in Figure 3a, a total of 94 warm-season RCDHEs are identified in the YRB from 1961 to 2024, with 868 OD and an average duration of 9.2 days. The interannual distribution shows notable year-to-year variability. Within-season distribution shows a bimodel structure with a pronounced peak in mid-July and a secondary peak in late September (Figure 3b), and nearly 71% of total OD of RCDHEs occurs between May and July.

During the warm seasons of 1961–2024, the OD of CDHEs at station scale increases from northeast to southwest, with significantly higher OD (>320 days) observed in south of the YRB (Figure 4a). For most of the YRB, the OD of CDHEs at station scale during the RCDHEs in warm season is more than 100 days, with a high center located along a southwest-northeast orientation in the central YRB (Figure 4b). The high OP (>24%) zones of CDHEs during the RCDHEs are concentrated in the southern, eastern, and western parts of the YRB, including eastern Sichuan, eastern Chongqing, and southern Anhui (Figure 4c). Notably, the contribution of RCDHEs to OD of CDHEs exceeds 45% across most of the YRB, with a high center reaching 60% over the central YRB (Figure 4d).

As shown in Figures 5a–5d, the regional mean intensity, CR, intensity, and OD of RCDHEs over the YRB in warm season all show significant increasing trends during the period of 1961–2024. In addition, an abrupt interdecadal shift around 2001 for the OD is identified by 10-year sliding *t*-test (not shown) with the regional mean intensity, OD and intensity increasing at a faster rate after 2000. The regional mean intensity of RCDHEs in Figure 5a shows a decreasing (increasing) trend of 0.131 (0.585) per decade during the period of 1961–2000 (2001–2024), which is contributed by the decreasing (increasing) trends of CR, intensity and OD (intensity and OD) of the RCDHEs shown in Figures 5b–5d. Moreover, Figures 5e–5h show 71.3% of RCDHEs with the regional mean intensity less than 0.4, 83% of RCDHEs with CR between 5% and 18%, 64.9% of the RCDHEs with intensity more than 0.25%, and 75.5% of RCDHEs with the duration ≤13 days.

3.2. Typical Synoptic Patterns Responsible for the RCDHEs Over the YRB in Warm Season and Features of RCDHEs Under Different Synoptic Patterns

According to the Calinski-Harabasz score, two dominant synoptic patterns named P1 and P2 driving the RCDHEs over the YRB in warm seasons are identified through spectral clustering method. As shown in Figures 6a and 6b, the P1 (P2) synoptic pattern occurs in 517 (351) days out of the 868 days of RCDHEs, contributing to 59.6%

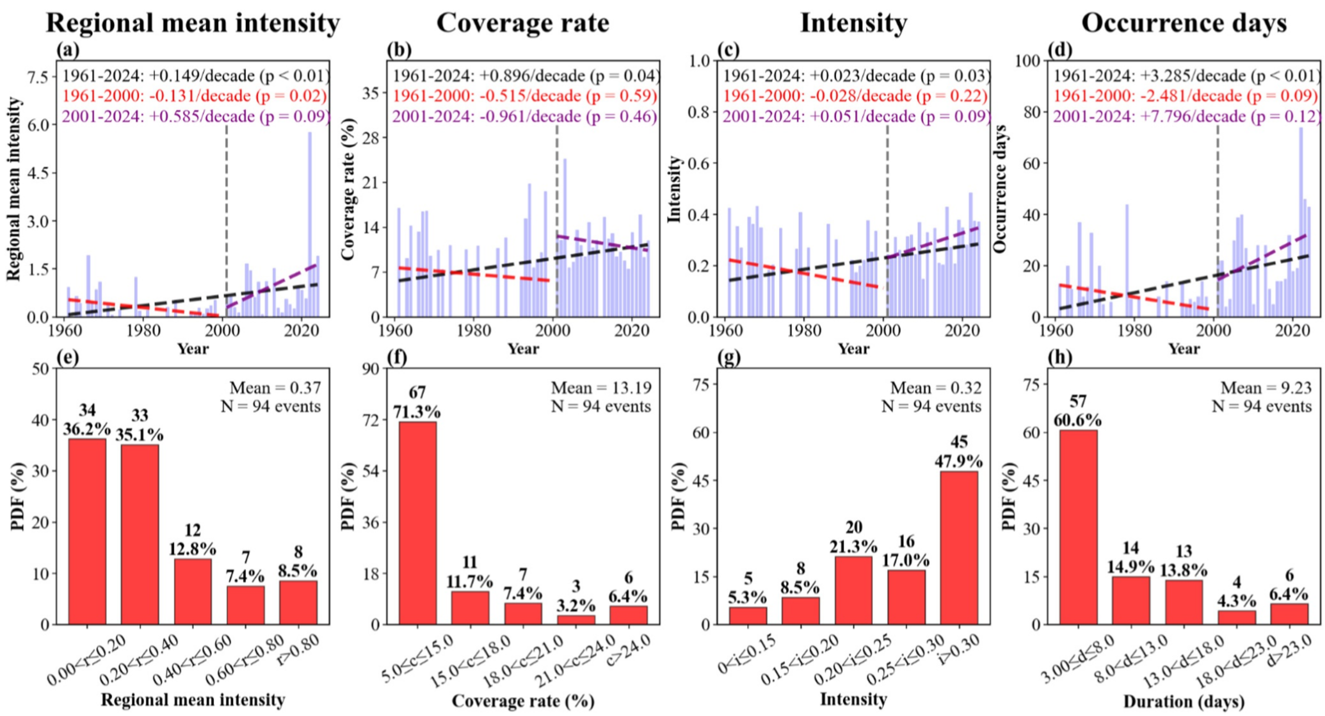

Figure 5. (a–d) Time series of annual mean regional mean intensity, coverage rate (CR), and intensity, and annual occurrence days of regional compound dry-hot events (RCDHEs) over the Yangtze River Basin in warm season during the period of 1961–2024. Black, red, and purple dashed lines indicate the linear trends for 1961–2024, 1961–2000, and 2001–2024, respectively, with the associated trends and *p*-values shown by the text in panels (a–d). The vertical gray dashed line marks 2001 which is identified as an abrupt change point by a 10-year sliding *t*-test. (e–h) Probability density functions for the regional mean intensity, CR, intensity, and duration of RCDHEs, respectively. The mean value and total number of RCDHEs are shown in the upper right corner of each panel.

(40.4%) occurrences of the RCDHEs. The P1 (P2) pattern features that the intensified WPSH and SAH with southerly (northerly) location relative to the climatology move toward each other (Figures 6a–6d). This is consistent with the high intensity and OP of CDHEs in the southern (central-eastern) YRB (Figures 6a–6d). In addition, the two synoptic patterns show distinct sub-seasonal variations (Figures 6e and 6f). The OD of RCDHEs under P1 during warm seasons of 1961–2024 concentrates in May-June and September-October, with a peak of 177 days in June (Figure 6e). And the OD of RCDHEs under the P2 pattern concentrates in July and August, with a peak of 224 days in July, accounting for 64% of the total OD under the P2 pattern during the warm seasons of 1961–2024 (Figure 6f).

The decreasing (increasing) trend in the regional mean intensity of RCDHEs in 1961–2000 (2001–2024) (Figure 5a) is mainly driven by the that of RCDHEs under the P1 pattern (Figure 7a). Specifically, under the P1 pattern, the decreasing (increasing) trend in the regional mean intensity of RCDHEs during the period of 1961–2000 (2001–2024) is associated with the decreases in the CR, intensity and OD (the increases in the intensity and OD) of RCDHEs (Figures 7a, 7c, 7e, and 7g). The accelerated increase in regional mean intensity and OD of RCDHEs after 2000 is primarily attributable to the P1 pattern, under which both the annual OD (+7.830 days/decade, $p = 0.048$) and regional mean intensity (+0.436/decade, $p = 0.017$) increase significantly after 2000, while the situations under the P2 pattern shows no significant trends in either metric after 2000 (Figures 7b and 7h). Moreover, the decreasing (increasing) trend in the regional mean intensity of RCDHEs during the period of 1961–2000 (2001–2024) is associated with the decreasing trends of the CR, intensity, and OD (the increasing trends of CR and intensity) of RCDHEs under the P2 pattern (Figures 7b, 7d, 7f, and 7h).

3.3. Physical Mechanisms of Warm-Season RCDHEs Under Different Synoptic Patterns

As shown in Figures 8a and 8b, anomalous water vapor divergence is mainly located over the southern (central-eastern) YRB under the P1 (P2) pattern, leading to moisture deficiency and the lack of favorable conditions for precipitation formation. Correspondingly, anomalous subsidence appears south of 30°N under the P1 synoptic pattern and north of 30°N under the P2 synoptic pattern (Figures 8c and 8d), consistent with the southward and

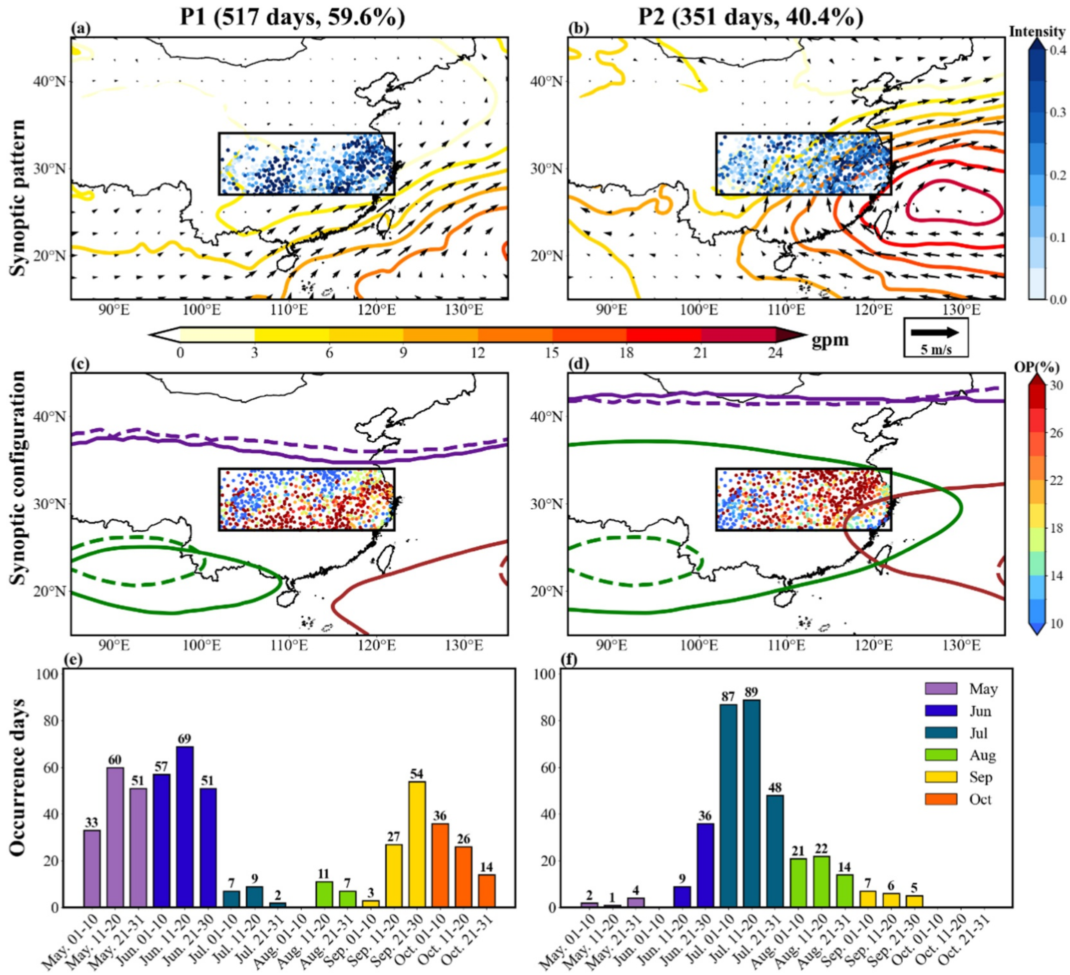

Figure 6. Circulation characteristics of the two dominant synoptic patterns (P1 and P2) responsible for the warm-season regional compound dry-hot events (RCDHEs) over the Yangtze River Basin during the period of 1961–2024. Spatial distribution of 850 hPa geopotential height anomaly (shaded) and wind anomaly field (vector) and the station-level intensity of RCDHEs (dots) under the P1 and P2 patterns, respectively (a–b). (c–d) show the composite mean South Asian high (SAH) at 200 hPa (green solid contour of 12,500 gpm) and the Western Pacific subtropical high (WPSH) at 500 hPa (brown solid contour of 5,880 gpm) during RCDHEs and the climatic mean of SAH and WPSH shown by the dashed lines with corresponding colors. The East Asian subtropical jet axis averaged during RCDHEs and its climatic mean are indicated by the purple solid and dashed lines shown in (c–d), respectively. In (c–d), the colored dots indicate the occurrence probability of compound dry-hot event at each station during the RCDHEs. Total occurrence days of RCDHEs in each 10 days from May to October during 1961–2024 under the P1 and P2 patterns, respectively (e–f).

northward shifts of the water vapor divergence center, respectively. This spatial distribution is also consistent with the high OP of RCDHEs under the two synoptic patterns (Figures 6c and 6d). In addition, anomalous subsidence dominates the whole YRB under both patterns along the longitudinal direction (102°–122°E), favoring the precipitation reduction over the YRB (Figures 8e and 8f).

Thermodynamic budget analysis shows that near-surface warming over the YRB during RCDHEs is mainly dominated by the vertical motion term z_mot, followed by the diabatic heating term DHT (Figures 9a and 9b). The zonal temperature advection term x_adv is negative under both patterns. The meridional temperature advection term y_adv is weakly positive under the P1 pattern (Figure 9a) but becomes negative under the P2 pattern (Figure 9b). Figures 9c–9f further show lower-tropospheric warm anomalies and anomalous subsidence under both patterns, with relatively stronger and deeper subsidence under the P2.

Under the P1 (P2) pattern, anomalous high pressure induces anomalous subsidence mainly over the southern (central-eastern) YRB (Figures 6a–6d). Correspondingly, both low cloud fraction (LCF) and precipitation

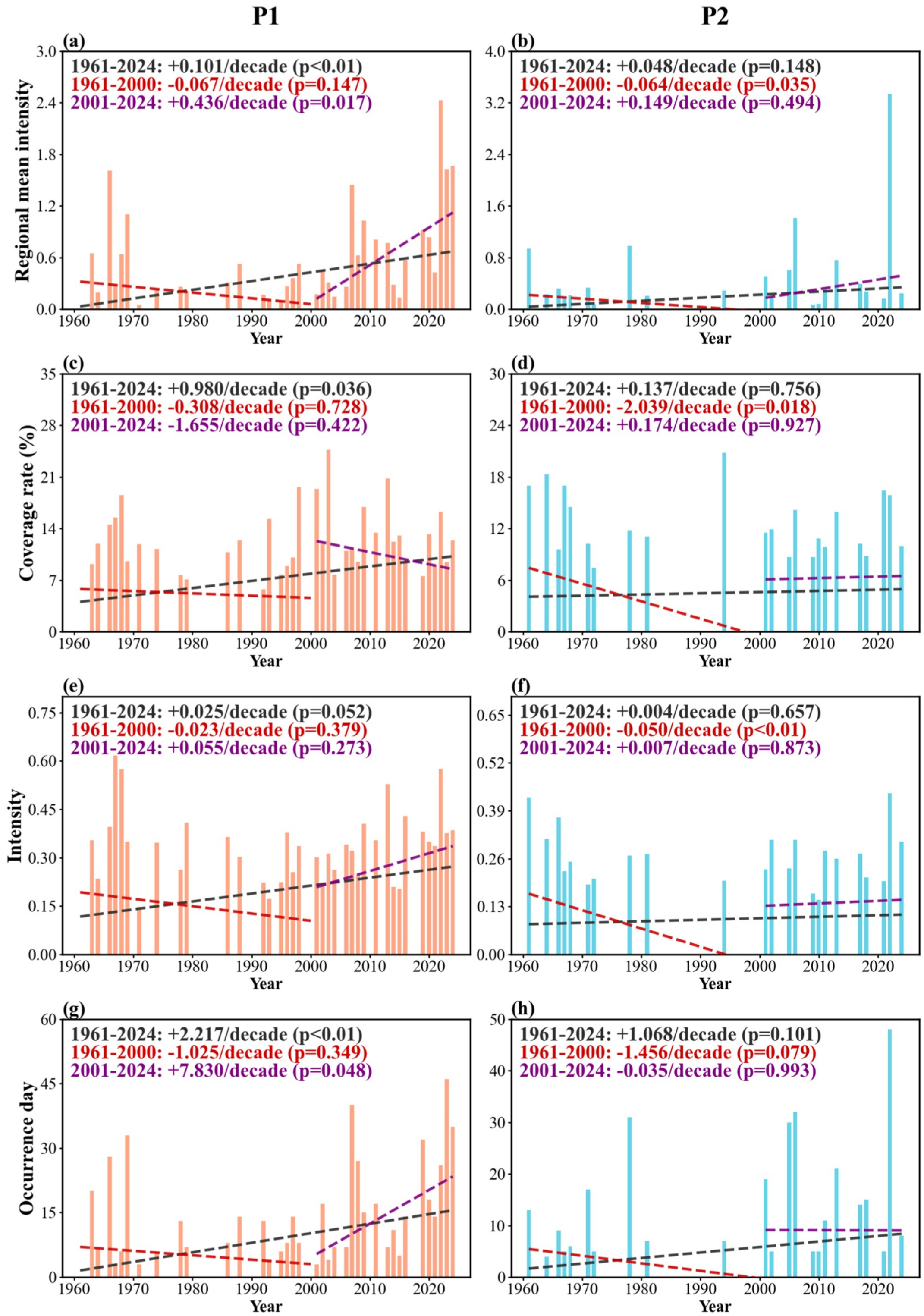

Figure 7. Time series of annual mean regional mean intensity, coverage rate, and intensity, and annual occurrence days of regional compound dry-hot events over the Yangtze River Basin in warm season during 1961–2024 under the P1 and P2 patterns. Black, red, and purple dashed lines indicate the linear trends for 1961–2024, 1961–2000, and 2001–2024 in each panel, respectively. The associated trends and *p*-values are shown by the text in each panel.

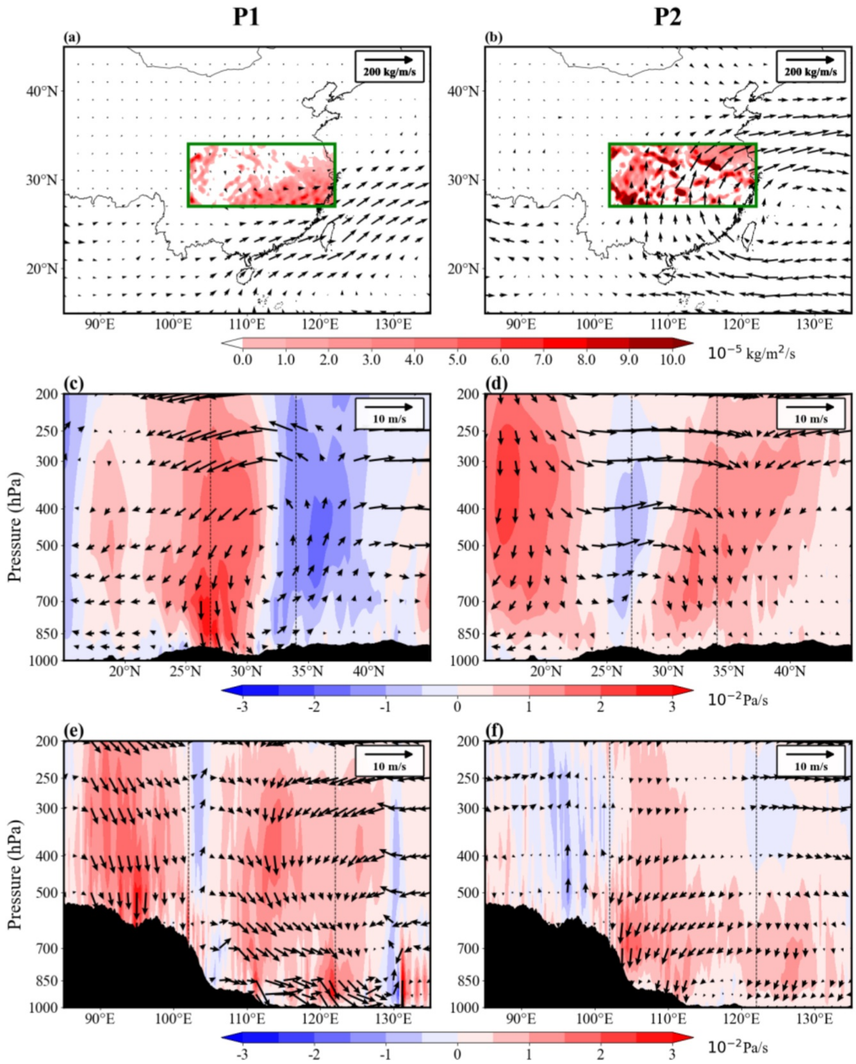

Figure 8. (a–b) The column-integrated (surface to 300 hPa) water vapor transport flux (vector) and its divergence anomalies (shaded) under P1 and P2 patterns, respectively. Positive values (red shadings) indicate water vapor divergence, calculated as $-\frac{1}{g}\int_{p_s}^{300} \nabla \cdot (q\mathbf{V})\, dp$, where g is gravitational acceleration (9.8 m·s^{-2}), p_s is surface pressure (Pa), q is specific humidity (kg·kg^{-1}), $\mathbf{V}$ is the horizontal wind vector (m·s^{-1}), and $\nabla\cdot$ denotes the horizontal divergence operator. (c–d) Pressure-latitude cross sections of vertical velocity anomalies (shaded) and meridional-vertical circulation anomalies (vector: meridional wind and vertical velocity × 100) averaged along 102°–122°E under the P1 and P2 patterns, respectively. (e–f) Pressure-longitude cross sections of vertical velocity anomalies (shaded) and zonal-vertical circulation anomalies (vector: zonal wind and vertical velocity × 100) averaged along 27°–34°N under the P1 and P2 patterns. Black shading represents the topography.

decrease over the southern (central-eastern) YRB under the P1 (P2) pattern (Figures 10c–10f). And the decrease in LCF increases the surface net shortwave radiation (NSR), leading to positive NSR anomalies over the southern (central-eastern) YRB under P1 (P2) pattern (Figures 10i and 10j), which further enhance the surface net radiation (Figures 10k and 10l) and promote near-surface warming (Figures 10a and 10b). Meanwhile, the land surface mainly transfers energy to the atmosphere through sensible heat flux (SH) heating (Figures 10g and 10h). Enhanced SH and suppressed precipitation suggest a shift in surface energy partitioning toward sensible heating, further amplifying increases of near surface daily maximal air temperature ($T_{\max}$) and reinforcing dry-hot conditions (Polychroni et al., 2025; Zscheischler et al., 2020). Overall, the reduced low cloud faction and precipitation under the P1 (P2) patterns enhance the NSR and surface heating over the southern (central-eastern) YRB, thereby increasing the likelihood of CDHEs there.

10.1029/2026JD047324

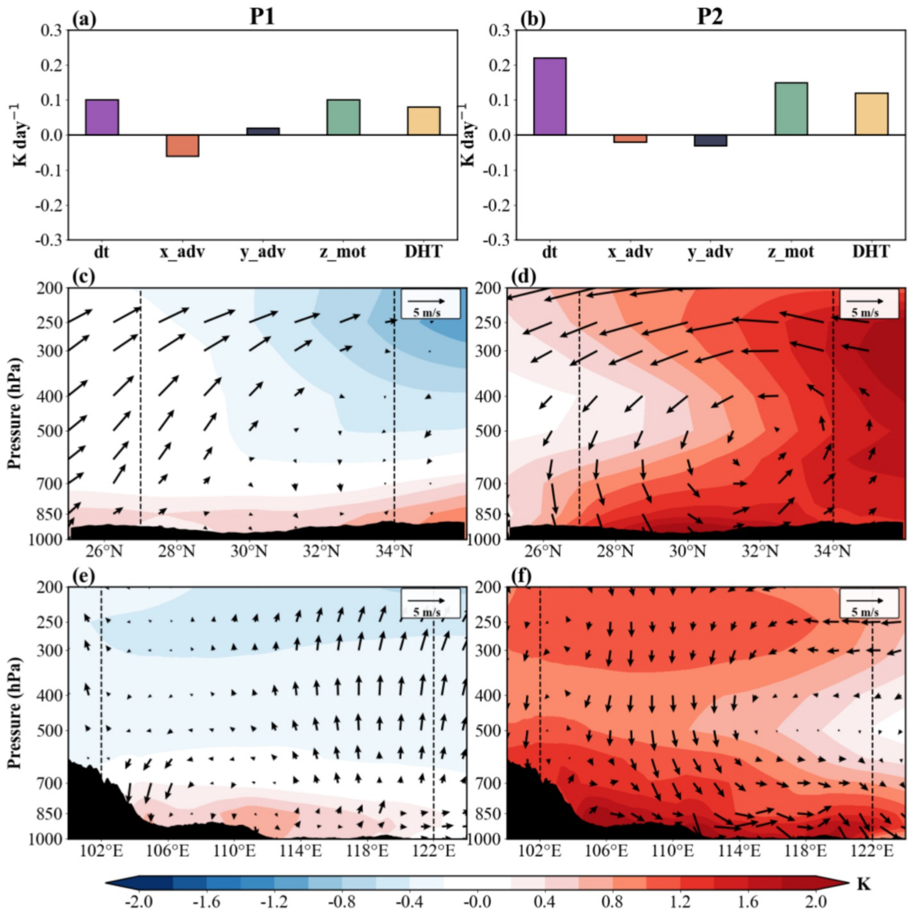

Figure 9. (a–b) The composite mean of each thermodynamic budget term in the near-surface during the regional compound dry-hot events (RCDHEs) under the P1 and P2 patterns regionally averaged over the Yangtze River Basin (YRB) during the period of 1961–2024. (c–d) The pressure-latitude cross-sections of the anomalous air temperature and circulation during the RCDHEs under the P1 and P2 patterns averaged along 102°–122°E relative to the climatic mean, respectively. (e–f) The pressure-longitude cross-sections of the anomalous air temperature and circulation during the RCDHEs under the P1 and P2 patterns averaged along 27°–34°N relative to the climatic mean, respectively. The YRB is marked by the black lines and the terrain is shown by black shading in panels (c–f).

4. Discussion

4.1. Daily-Scale Identification Advances Understanding of Evolution of RCDHEs

Previous studies on CDHEs over the YRB have mainly focused on individual extreme events or monthly-scale statistics (S. Tang et al., 2023; Yuan et al., 2024). By developing a daily-scale CDHMI, this study provides a process-oriented method for identifying RCDHEs consistently over 1961–2024. Compared with monthly approaches, the daily scale better captures the co-evolution of drought and heat at synoptic time scales and therefore characterizes the occurrence, intensity, and persistence of RCDHEs more realistically. The significant post-2000 increase in RCDHE intensity and OD is consistent with previous studies reporting intensified compound hot-dry extremes under recent warming (Mukherjee et al., 2023; Tripathy et al., 2023). More importantly, our results further demonstrate that these long-term changes are closely linked to changes in dominant synoptic circulation regimes, providing a process-based perspective beyond previous event- or monthly-scale analyses.

4.2. Synoptic Circulation Regimes Explain the Recent Intensification of RCDHEs

This study identifies two dominant circulation regimes associated with warm-season RCDHEs over the YRB. The P1 circulation pattern closely resembles the large-scale configuration during the record-breaking 2022 event (Huang et al., 2024; Jiang et al., 2023), suggesting that the 2022 event represents an extreme realization of a

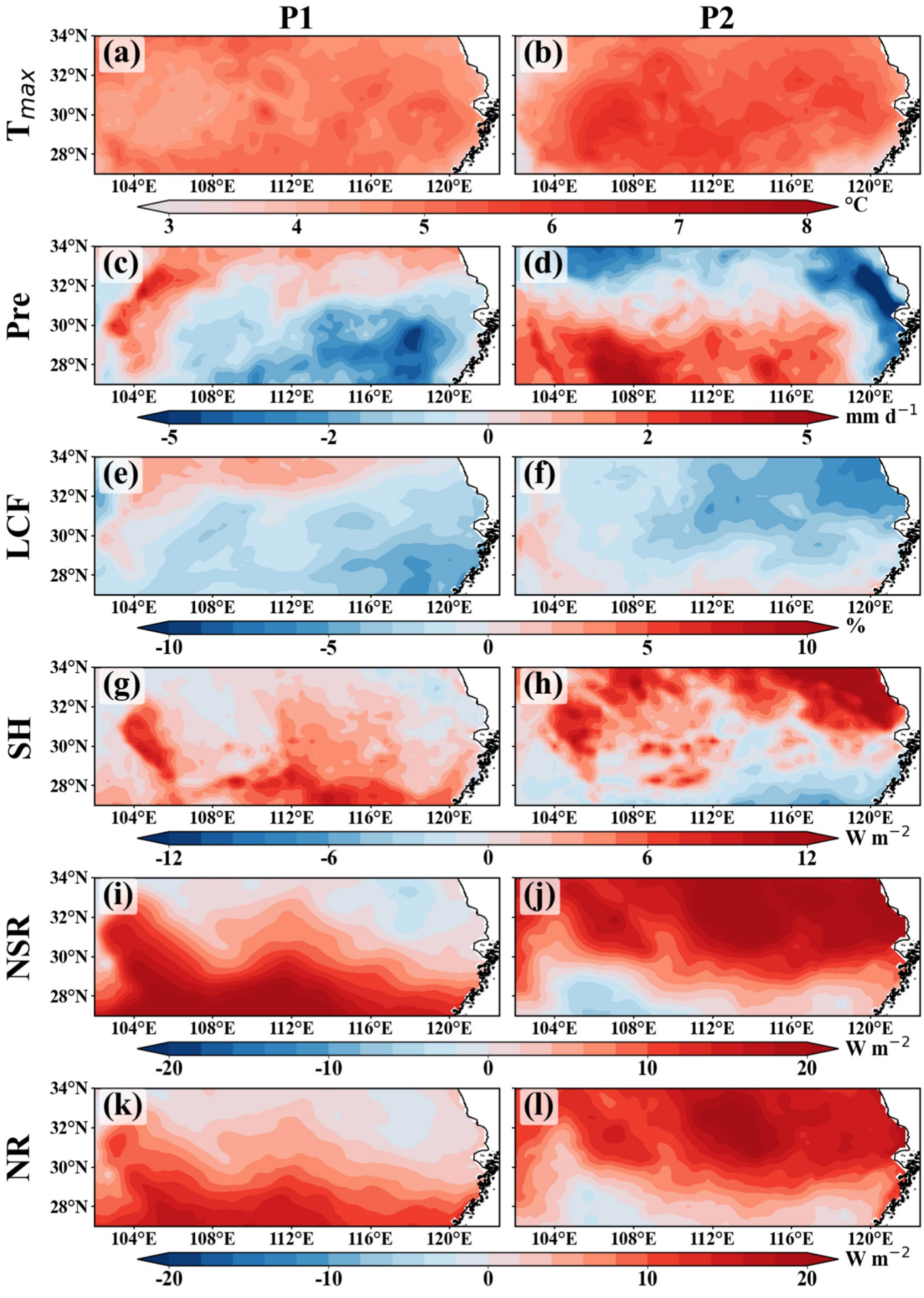

Figure 10. The anomalies of daily maximum temperature (T_{max}), precipitation (Pre), low cloud fraction, sensible heat flux (SH), surface net shortwave radiation and surface net radiation over the Yangtze River Basin during the regional compound dry-hot events under the P1 and P2 synoptic patterns relative to the climatic mean of 1961–2024, respectively.

circulation regime that has become increasingly frequent after 2000 rather than an isolated anomaly. Mechanism analysis further shows that anomalous subsidence, reduced cloud cover, enhanced net surface radiation, and increased sensible heat flux jointly reinforce regional warming and drying under both patterns. These results agree with previous studies, highlighting the importance of land-atmosphere feedbacks in sustaining compound drought-heat extremes (Dirmeyer et al., 2021; Hirsch et al., 2019; Ni et al., 2024). The dominant contribution of the P1 pattern further indicates that circulation changes have become an important driver of the recent intensification of RCDHEs over the YRB.

4.3. Implications and Future Perspectives

The circulation-based framework developed here has important implications for climate prediction and impact assessment (Grams et al., 2017; White et al., 2022). Because the two circulation patterns exhibit distinct seasonal preferences and spatial influence regions, monitoring large-scale circulation anomalies may improve subseasonal prediction of RCDHEs (Hao et al., 2022; Yuan et al., 2023). The contrasting spatial distributions of the two patterns also imply different ecosystem vulnerabilities across the YRB, suggesting that future ecological assessments should explicitly consider circulation-dependent drought-heat interactions (Liang et al., 2015; A. Wang et al., 2024). Nevertheless, this study mainly focuses on atmospheric circulation and meteorological conditions. The respective contributions of soil moisture, vegetation dynamics, and anthropogenic forcing remain to be quantified (Shi et al., 2026; Z. Wang et al., 2025). Future work combining land surface models and ecosystem observations will help further clarify the nonlinear interactions between circulation anomalies, land-atmosphere feedbacks, and ecosystem responses.

5. Conclusion

This study established a daily-scale framework for identifying warm-season RCDHEs over the YRB by integrating the SPI30 with the 90th percentile threshold of daily maximum temperature through the CDHMI. Based on daily observations from 639 meteorological stations during 1961–2024, the long-term characteristics, interdecadal changes, dominant synoptic circulation patterns, and associated physical mechanisms of RCDHEs were systematically investigated. The major conclusions are summarized as follows:

A total of 94 warm-season RCDHEs were identified during 1961–2024, accounting for more than 45% of all warm-season CDHE OD in most YRB. RCDHEs exhibited pronounced subseasonal variability, with the highest occurrence frequency from mid-June to mid-July. The CR, OD, and regional mean intensity of RCDHEs all showed significant increasing trends over the past 60 years. A distinct interdecadal transition occurred around 2000, after which the OD and intensity increased much more rapidly, indicating a substantial intensification of regional compound dry-hot hazards under recent climate warming.

Spectral clustering objectively identified two dominant synoptic circulation patterns responsible for the warm-season RCDHEs. The P1 pattern is characterized by an intensified and southward-displaced WPSH and SAH, whereas the P2 pattern exhibits a relatively northward circulation configuration. The two patterns show distinct seasonal preferences and spatial influence regions. Trend attribution further demonstrates that the accelerated increasing rate of intensity of RCDHES after 2000 is primarily associated with enhanced occurrence and persistence of the P1 pattern, highlighting the dominant role of large-scale circulation changes in regulating the long-term evolution of regional compound dry-hot extremes.

Mechanism analysis indicates that both circulation patterns promote the development of RCDHEs through similar physical processes, including anomalous subsidence, reduced cloud cover and precipitation, enhanced net surface radiation, and increased upward sensible heat flux at surface. These processes jointly strengthen land-atmosphere feedbacks, favor concurrent drought and heat conditions, and ultimately increase the occurrence frequency and intensity of RCDHEs. Although the strongest anomalies occur over different parts of the YRB under the two circulation patterns, their thermodynamic effects consistently reinforce regional warming and drying, providing new insights into the circulation dependence of warm-season RCDHEs over the YRB.

Conflict of Interest

The authors declare no conflicts of interest relevant to this study.

Availability Statement

The daily surface meteorological station observations over China used in this study are provided by the China Meteorological Administration (CMA, 2023). The ERA5 hourly reanalysis data on pressure levels are available from Hersbach et al. (2023).

Acknowledgments
This study is supported by the National Natural Science Foundation of China under Grant U2342207, the Jiangsu Province Postgraduate Research Innovation Program under Grant 26CXJH0255, and the Jiangsu Collaborative Innovation Center for Climate Change. We appreciate the High Performance Computing Center of Nanjing University.

References

AghaKouchak, A., Chiang, F., Huning, L. S., Love, C. A., Mallakpour, I., Mazdiyasni, O., et al. (2020). Climate extremes and compound hazards in a warming world. *Annual Review of Earth and Planetary Sciences*, *48*(1), 519–548. https://doi.org/10.1146/annurev-earth-071719-055228

Albers, J. R., & Newman, M. (2021). Subseasonal predictability of the North Atlantic oscillation. *Environmental Research Letters*, *16*(4), 044024. https://doi.org/10.1088/1748-9326/abe781

Alizadeh, M. R., Adamowski, J., Nikoo, M. R., AghaKouchak, A., Dennison, P., & Sadegh, M. (2020). A century of observations reveals increasing likelihood of continental-scale compound dry-hot extremes. *Science Advances*, *6*(39), eaaz4571. https://doi.org/10.1126/sciadv.aaz4571

An, N., Chen, Y., Liao, Z., & Li, J. (2025). Trans-seasonal vegetation-land-atmosphere interactions explained record-breaking cascading extremes in the upper reaches of the Yangtze River. *Geophysical Research Letters*, *52*(10), e2024GL114165. https://doi.org/10.1029/2024GL114165

Ayarzagüena, B., Ineson, S., Dunstone, N. J., Baldwin, M. P., & Scaife, A. A. (2018). Intraseasonal effects of El Niño–Southern Oscillation on North Atlantic climate. *Journal of Climate*, *31*(21), 8861–8873. https://doi.org/10.1175/JCLI-D-18-0097.1

Bevacqua, E., Suarez-Gutierrez, L., Jézéquel, A., Lehner, F., Vrac, M., Yiou, P., & Zscheischler, J. (2023). Advancing research on compound weather and climate events via large ensemble model simulations. *Nature Communications*, *14*(1), 2145. https://doi.org/10.1038/s41467-023-37847-5

Bjerre, E., Jessen, S., Schneider, R., Villholth, K. G., Dippenaar, M. A., Enemark, T., et al. (2026). Groundwater responses to decadal rainfall variability in semi-arid South Africa. *Journal of Hydrology*, *669*, 135022. https://doi.org/10.1016/j.jhydrol.2026.135022

Caliński, T., & Harabasz, J. (1974). A dendrite method for cluster analysis. *Communications in Statistics - Theory and Methods*, *3*, 1–27. https://doi.org/10.1080/03610927408827101

Chen, D., Qiao, S., Yang, J., Tang, S., Zuo, D., & Feng, G. (2024). Contribution of anthropogenic influence to the 2022-like Yangtze River valley compound heatwave and drought event. *npj Climate and Atmospheric Science*, *7*(1), 172. https://doi.org/10.1038/s41612-024-00720-3

Chen, H., & Sun, J. (2015). Assessing model performance of climate extremes in China: An intercomparison between CMIP5 and CMIP3. *Climatic Change*, *129*(1–2), 197–211. https://doi.org/10.1007/s10584-014-1319-5

Chen, X., Wang, J., Pan, F., Song, Y., Liang, J., Huang, N., et al. (2025). Land-atmosphere feedback exacerbated the mega heatwave and drought over the Yangtze River Basin of China during summer 2022. *Agricultural and Forest Meteorology*, *361*, 110321. https://doi.org/10.1016/j.agrformet.2024.110321

CMA (China Meteorological Administration). (2023). Daily data set of Chinese surface climatological data (V3.0) [Dataset]. *National Meteorological Information Centre (NMIC)*. Retrieved from http://data.cma.cn

Ding, R., Ha, K.-J., & Li, J. (2010). Interdecadal shift in the relationship between the East Asian summer monsoon and the tropical Indian Ocean. *Climate Dynamics*, *34*(7–8), 1059–1071. https://doi.org/10.1007/s00382-009-0555-2

Ding, T., Qian, W., & Yan, Z. (2010). Changes in hot days and heat waves in China during 1961–2007. *International Journal of Climatology*, *30*(10), 1452–1462. https://doi.org/10.1002/joc.1989

Ding, Y., Ren, G., Zhao, Z., Xu, Y., Luo, Y., Li, Q., & Zhang, J. (2007). Detection, causes and projection of climate change over China: An overview of recent progress. *Advances in Atmospheric Sciences*, *24*(6), 954–971. https://doi.org/10.1007/s00376-007-0954-4

Ding, Y., Wang, Z., & Sun, Y. (2008). Inter-decadal variation of the summer precipitation in East China and its association with decreasing Asian summer monsoon. Part I: Observed evidences. *International Journal of Climatology: A Journal of the Royal Meteorological Society*, *28*(9), 1139–1161. https://doi.org/10.1002/joc.1615

Dirmeyer, P. A., Balsamo, G., Blyth, E. M., Morrison, R., & Cooper, H. M. (2021). Land-Atmosphere interactions exacerbated the drought and heatwave over Northern Europe during summer 2018. *AGU Advances*, *2*, e2020AV000283. https://doi.org/10.1029/2020AV000283

Domeisen, D. I., White, C. J., Afargan-Gerstman, H., Muñoz, Á. G., Janiga, M. A., Vitart, F., et al. (2022). Advances in the subseasonal prediction of extreme events: Relevant case studies across the globe. *Bulletin of the American Meteorological Society*, *103*(6), E1473–E1501. https://doi.org/10.1175/BAMS-D-20-0221.1

Donath, W. E., & Hoffman, A. J. (1973). Lower bounds for the partitioning of graphs. *IBM Journal of Research and Development*, *17*(5), 420–425. https://doi.org/10.1147/rd.175.0420

Feng, S., Gu, X., Guan, Y., Wang, Q. J., Wang, L., Du, L., et al. (2025). Anthropogenic exacerbations of summer-autumn compound dry-hot severity in the middle and lower reaches of the Yangtze River. *Journal of Hydrology*, *646*, 132346. https://doi.org/10.1016/j.jhydrol.2024.132346

Feng, S., Gu, X., Guan, Y., Wang, Q. J., Zheng, Y., Wang, L., et al. (2024). Anthropogenic exacerbation in dry-hot probability and consequential record-shattering droughts in the middle and lower reaches of the Yangtze River. *Journal of Geophysical Research: Atmospheres*, *129*(20), e2024JD041603. https://doi.org/10.1029/2024JD041603

Fischer, E. M., Seneviratne, S. I., Vidale, P. L., Lüthi, D., & Schär, C. (2007). Soil moisture–atmosphere interactions during the 2003 European summer heat wave. *Journal of Climate*, *20*, 5081–5099. https://doi.org/10.1175/JCLI4288.1

Ford, T. W., & Labosier, C. F. (2017). Meteorological conditions associated with the onset of flash drought in the eastern United States. *Agricultural and Forest Meteorology*, *247*, 414–423. https://doi.org/10.1016/j.agrformet.2017.08.031

Fu, K., & Wang, K. (2023). Contributions of local land–atmosphere coupling and mesoscale atmospheric circulation to the 2013 extreme flash drought and heatwave compound event over southwest China. *Journal of Geophysical Research: Atmospheres*, *128*(21), e2023JD039406. https://doi.org/10.1029/2023JD039406

Ge, J., You, Q., & Zhang, Y. (2019). Effect of Tibetan Plateau heating on summer extreme precipitation in eastern China. *Atmospheric Research*, *218*, 364–371. https://doi.org/10.1016/j.atmosres.2018.12.018

Gibson, P. B., Chapman, W. E., Altinok, A., Delle Monache, L., DeFlorio, M. J., & Waliser, D. E. (2021). Training machine learning models on climate model output yields skillful interpretable seasonal precipitation forecasts. *Communications Earth & Environment*, *2*(1), 159. https://doi.org/10.1038/s43247-021-00225-4

Grams, C. M., Beerli, R., Pfenninger, S., Staffell, I., & Wernli, H. (2017). Balancing Europe's wind-power output through spatial deployment informed by weather regimes. *Nature Climate Change*, *7*(8), 557–562. https://doi.org/10.1038/nclimate3338

Guo, J., Su, T., Li, Z., Miao, Y., Li, J., Liu, H., et al. (2017). Declining frequency of summertime local-scale precipitation over eastern China from 1970 to 2010 and its potential link to aerosols. *Geophysical Research Letters*, *44*(11), 5700–5708. https://doi.org/10.1002/2017GL073533

Hao, Z., Hao, F., Xia, Y., Feng, S., Sun, C., Zhang, X., et al. (2022). Compound droughts and hot extremes: Characteristics, drivers, changes, and impacts. *Earth-Science Reviews*, *235*, 104241. https://doi.org/10.1016/j.earscirev.2022.104241

Hersbach, H., Bell, B., Berrisford, P., Biavati, G., Horányi, A., Muñoz Sabater, J., et al. (2023). ERA5 hourly data on pressure levels from 1940 to present [Dataset]. *Copernicus Climate Change Service (C3S) Climate Data Store (CDS)*. https://doi.org/10.24381/cds.bd0915c6

Hersbach, H., Bell, B., Berrisford, P., Hirahara, S., Horányi, A., Muñoz-Sabater, J., et al. (2020). The ERA5 global reanalysis. *Quarterly Journal of the Royal Meteorological Society*, *146*(730), 1999–2049. https://doi.org/10.1002/qj.3803

Hirsch, A. L., Evans, J. P., Di Virgilio, G., Perkins-Kirkpatrick, S. E., Argüeso, D., Pitman, A. J., et al. (2019). Amplification of Australian heatwaves via local land-atmosphere coupling. *Journal of Geophysical Research: Atmospheres*, *124*(24), 13625–13647. https://doi.org/10.1029/2019JD030665

Huang, H., Zhu, Z., & Li, J. (2024). Disentangling the unprecedented Yangtze River basin extreme high temperatures in summer 2022: Combined impacts of the reintensified La Niña and strong positive NAO. *Journal of Climate*, *37*(3), 927–942. https://doi.org/10.1175/JCLI-D-23-0466.1

Huth, R., Beck, C., Philipp, A., Demuzere, M., Ustrnul, Z., Cahynová, M., et al. (2008). Classifications of atmospheric circulation patterns: Recent advances and applications. *Annals of the New York Academy of Sciences*, *1146*(1), 105–152. https://doi.org/10.1196/annals.1446.019

Jiang, J., Liu, Y., Mao, J., & Wu, G. (2023). Extreme heatwave over Eastern China in summer 2022: The role of three oceans and local soil moisture feedback. *Environmental Research Letters*, *18*(4), 044025. https://doi.org/10.1088/1748-9326/acc5fb

Jouan, G., Cuzol, A., Monbet, V., & Monnier, G. (2023). Gaussian mixture models for clustering and calibration of ensemble weather forecasts. *Discrete and Continuous Dynamical Systems - Series S*, *16*(2), 1.

Kong, Q., Guerreiro, S. B., Blenkinsop, S., Li, X. F., & Fowler, H. J. (2020). Increases in summertime concurrent drought and heatwave in Eastern China. *Weather and Climate Extremes*, *28*, 100242. https://doi.org/10.1016/j.wace.2019.100242

Kornhuber, K., Coumou, D., Vogel, E., Lesk, C., Donges, J. F., Lehmann, J., & Horton, R. M. (2020). Amplified Rossby waves enhance risk of concurrent heatwaves in major breadbasket regions. *Nature Climate Change*, *10*(1), 48–53. https://doi.org/10.1038/s41558-019-0637-z

Lee, Y., Wenig, M., & Chan, K. (2023). Oceanic and atmospheric anomalies associated with extreme precipitation events in China 1983–2020. *Air Quality, Atmosphere & Health*, *16*(5), 881–895. https://doi.org/10.1007/s11869-022-01295-9

Leonard, M., Westra, S., Phatak, A., Lambert, M., van den Hurk, B., McInnes, K., et al. (2014). A compound event framework for understanding extreme impacts. *Wiley Interdisciplinary Reviews: Climate Change*, *5*(1), 113–128. https://doi.org/10.1002/wcc.252

Li, Y., Xu, H., & Liu, D. (2011). Features of the extremely severe drought in the east of Southwest China and anomalies of atmospheric circulation in summer 2006. *Acta Meteorologica Sinica*, *25*(2), 176–187. https://doi.org/10.1007/s13351-011-0025-8

Liang, W., Yang, Y., Fan, D., Guan, H., Zhang, T., Long, D., et al. (2015). Analysis of spatial and temporal patterns of net primary production and their climate controls in China from 1982 to 2010. *Agricultural and Forest Meteorology*, *204*, 22–36. https://doi.org/10.1016/j.agrformet.2015.01.015

Liu, J., & Han, J. (2018). Spectral clustering. In *Data clustering* (pp. 177–200). Chapman and Hall/CRC.

Liu, W., Shi, N., Wang, H., & Huang, Q. (2024). Thermodynamic characteristics of extreme heat waves over the middle and lower reaches of the Yangtze River Basin. *Climate Dynamics*, *62*(5), 3877–3889. https://doi.org/10.1007/s00382-024-07104-6

Liu, Y., Huang, D., Zhu, J., & Cheng, C. S. (2023). The quadrupole precipitation pattern over eastern China and its associated atmospheric circulations and ocean conditions. *Journal of Climate*, *36*(18), 6561–6575. https://doi.org/10.1175/JCLI-D-22-0075.1

Liu, Y., Yuan, S., Zhu, Y., Ren, L., Chen, R., Zhu, X., & Xia, R. (2023). The patterns, magnitude, and drivers of unprecedented 2022 mega-drought in the Yangtze River Basin, China. *Environmental Research Letters*, *18*(11), 114006. https://doi.org/10.1088/1748-9326/acfe21

Luo, M., & Lau, N. C. (2018). Increasing heat stress in urban areas of eastern China: Acceleration by urbanization. *Geophysical Research Letters*, *45*(23), 13060–13069. https://doi.org/10.1029/2018GL080306

Mamalakis, A., Barnes, E. A., & Ebert-Uphoff, I. (2022). Investigating the fidelity of explainable artificial intelligence methods for applications of convolutional neural networks in geoscience. *Artificial Intelligence for the Earth Systems*, *1*(4), e220012. https://doi.org/10.1175/AIES-D-22-0012.1

Manning, C., Widmann, M., Bevacqua, E., Van Loon, A. F., Maraun, D., & Vrac, M. (2018). Soil moisture drought in Europe: A compound event of precipitation and potential evapotranspiration on multiple time scales. *Journal of Hydrometeorology*, *19*(8), 1255–1271. https://doi.org/10.1175/JHM-D-18-0017.1

McKee, T. B., Doesken, N. J., & Kleist, J. (1993). The relationship of drought frequency and duration to time scales. In *Paper presented at Proceedings of the 8th Conference on Applied Climatology, California*.

Miralles, D. G., Gentine, P., Seneviratne, S. I., & Teuling, A. J. (2019). Land–atmospheric feedbacks during droughts and heatwaves: State of the science and current challenges. *Annals of the New York Academy of Sciences*, *1436*(1), 19–35. https://doi.org/10.1111/nyas.13912

Mukherjee, S., & Mishra, A. K. (2021). Increase in compound drought and heatwaves in a warming world. *Geophysical Research Letters*, *48*(1), e2020GL090617. https://doi.org/10.1029/2020GL090617

Mukherjee, S., Mishra, A. K., Zscheischler, J., & Entekhabi, D. (2023). Interaction between dry and hot extremes at a global scale using a cascade modeling framework. *Nature Communications*, *14*(1), 277. https://doi.org/10.1038/s41467-022-35748-7

Ni, Y., Qiu, B., Miao, X., Li, L., Chen, J., Tian, X., et al. (2024). Shift of soil moisture-temperature coupling exacerbated 2022 compound hot-dry event in eastern China. *Environmental Research Letters*, *19*(1), 014059. https://doi.org/10.1088/1748-9326/ad178c

Ning, L., Liu, J., & Wang, B. (2017). How does the South Asian high influence extreme precipitation over eastern China? *Journal of Geophysical Research: Atmospheres*, *122*(8), 4281–4298. https://doi.org/10.1002/2016JD026075

Niu, Y., Ma, H., Han, T., & Chen, H. (2026). Improving seasonal prediction skill for South China heatwaves based on circulation classification and machine learning. *Atmospheric and Oceanic Science Letters*, 100812. https://doi.org/10.1016/j.aosl.2026.100812

Pendergrass, A. G., Meehl, G. A., Pulwarty, R., Hobbins, M., Hoell, A., AghaKouchak, A., et al. (2020). Flash droughts present a new challenge for subseasonal-to-seasonal prediction. *Nature Climate Change*, *10*(3), 191–199. https://doi.org/10.1038/s41558-020-0709-0

Pfahl, S., & Wernli, H. (2012). Quantifying the relevance of atmospheric blocking for co-located temperature extremes in the Northern Hemisphere on (sub-) daily time scales. *Geophysical Research Letters*, *39*(12), L12807. https://doi.org/10.1029/2012GL052261

Philipp, A., Bartholy, J., Beck, C., Erpicum, M., Esteban, P., Fettweis, X., et al. (2010). Cost733cat–A database of weather and circulation type classifications. *Physics and Chemistry of the Earth, Parts A/B/C*, *35*(9–12), 360–373. https://doi.org/10.1016/j.pce.2009.12.010

Polychroni, I. D., Nastos, P. T., Hatzaki, M., & Kapsomenakis, J. (2025). Compound extremes of air temperature and precipitation over the Mediterranean region. Understanding the influence of atmospheric circulation. *Atmospheric Research*, *330*, 108529. https://doi.org/10.1016/j.atmosres.2025.108529

Prodregosa, F. (2011). Scikit-learn: Machine learning in Python. *Journal of Machine Learning Research*, *12*, 2825–2830.

Raymond, C., Horton, R. M., Zscheischler, J., Martius, O., AghaKouchak, A., Balch, J., et al. (2020). Understanding and managing connected extreme events. *Nature Climate Change*, *10*(7), 611–621. https://doi.org/10.1038/s41558-020-0790-4

Ridder, N. N., Pitman, A. J., Westra, S., Ukkola, A., Do, H. X., Bador, M., et al. (2020). Global hotspots for the occurrence of compound events. *Nature Communications*, *11*(1), 5956. https://doi.org/10.1038/s41467-020-19639-3

Russo, S., Dosio, A., Graversen, R. G., Sillmann, J., Carrao, H., Dunbar, M. B., et al. (2014). Magnitude of extreme heat waves in present climate and their projection in a warming world. *Journal of Geophysical Research: Atmospheres*, *119*(22), 12500–12512. https://doi.org/10.1002/2014jd022098

Russo, S., Sillmann, J., & Fischer, E. M. (2015). Top ten European heatwaves since 1950 and their occurrence in the coming decades. *Environmental Research Letters*, *10*(12), 124003. https://doi.org/10.1088/1748-9326/10/12/124003

Salcedo-Sanz, S., Pérez-Aracil, J., Ascenso, G., Del Ser, J., Casillas-Pérez, D., Kadow, C., et al. (2024). Analysis, characterization, prediction, and attribution of extreme atmospheric events with machine learning and deep learning techniques: A review. *Theoretical and Applied Climatology*, *155*(1), 1–44. https://doi.org/10.1007/s00704-023-04571-5

Sassi, R. H., Dardouri, W., Yahmed, M. H., Gmada, N., Mahfoudhi, M. E., & Gharbi, Z. (2009). Relative and absolute reliability of a modified agility T-test and its relationship with vertical jump and straight sprint. *The Journal of Strength & Conditioning Research*, *23*(6), 1644–1651. https://doi.org/10.1519/JSC.0b013e3181b425d2

Schumacher, D. L., Keune, J., Van Heerwaarden, C. C., Vilà-Guerau de Arellano, J., Teuling, A. J., & Miralles, D. G. (2019). Amplification of mega-heatwaves through heat torrents fuelled by upwind drought. *Nature Geoscience*, *12*(9), 712–717. https://doi.org/10.1038/s41561-019-0431-6

Seneviratne, S. I., Zhang, X., Adnan, M., Badi, W., Dereczynski, C., Luca, A. D., et al. (2021). *Weather and climate extreme events in a changing climate* (pp. 1513–1766). Cambridge University Press. https://doi.org/10.1017/9781009157896.013

Sheffield, J., Andreadis, K., Wood, E. F., & Lettenmaier, D. (2009). Global and continental drought in the second half of the twentieth century: Severity–area–duration analysis and temporal variability of large-scale events. *Journal of Climate*, *22*(8), 1962–1981. https://doi.org/10.1175/2008JCLI2722.1

Shi, G., Wei, D., Qi, M., Zhang, Z., Niu, H., Zhang, Y., & Wang, B. (2026). Frequent dry–hot extremes slow the loss of semi-arid ecosystem resilience. *Global Change Biology*, *32*(4), e70835. https://doi.org/10.1111/gcb.70835

Si, D., & Ding, Y. (2016). Oceanic forcings of the interdecadal variability in East Asian summer rainfall. *Journal of Climate*, *29*(21), 7633–7649. https://doi.org/10.1175/JCLI-D-15-0792.1

Singh, J., Ashfaq, M., Skinner, C. B., Anderson, W. B., Mishra, V., & Singh, D. (2022). Enhanced risk of concurrent regional droughts with increased ENSO variability and warming. *Nature Climate Change*, *12*(2), 163–170. https://doi.org/10.1038/s41558-021-01276-3

Sippel, S., Meinshausen, N., Fischer, E. M., Székely, E., & Knutti, R. (2020). Climate change now detectable from any single day of weather at global scale. *Nature Climate Change*, *10*(1), 35–41. https://doi.org/10.1038/s41558-019-0666-7

Sun, Y., Zhang, X., Zwiers, F. W., Song, L., Wan, H., Hu, T., et al. (2014). Rapid increase in the risk of extreme summer heat in Eastern China. *Nature Climate Change*, *4*(12), 1082–1085. https://doi.org/10.1038/nclimate2410

Sutanto, S. J., Syaehuddin, W. A., & de Graaf, I. (2024). Hydrological drought forecasts using precipitation data depend on catchment properties and human activities. *Communications Earth & Environment*, *5*(1), 118. https://doi.org/10.1038/s43247-024-01295-w

Tang, S., Qiao, S., Wang, B., Liu, F., Feng, T., Yang, J., et al. (2023). Linkages of unprecedented 2022 Yangtze River Valley heatwaves to Pakistan flood and triple-dip La Niña. *npj Climate and Atmospheric Science*, *6*(1), 44. https://doi.org/10.1038/s41612-023-00386-3

Tang, Y., Huang, A., Wu, P., Huang, D., Xue, D., & Wu, Y. (2021). Drivers of summer extreme precipitation events over East China. *Geophysical Research Letters*, *48*(11), e2021GL093670. https://doi.org/10.1029/2021GL093670

Teng, H., & Branstator, G. (2019). Amplification of waveguide teleconnections in the boreal summer. *Current Climate Change Reports*, *5*(4), 421–432. https://doi.org/10.1007/s40641-019-00150-x

Thom, H. C. S. (1958). A note on the gamma distribution. *Monthly Weather Review*, *86*(4), 117–122. https://doi.org/10.1175/1520-0493(1958)086<0117:anotgd>2.0.co;2

Toms, B. A., Barnes, E. A., & Ebert-Uphoff, I. (2020). Physically interpretable neural networks for the geosciences: Applications to Earth system variability. *Journal of Advances in Modeling Earth Systems*, *12*(9), e2019MS002002. https://doi.org/10.1029/2019MS002002

Toreti, A., Bavera, D., Acosta Navarro, J., Cammalleri, C., De Jager, A., Di Ciollo, C., et al. (2022). *Drought in Europe August 2022*. Publications Office of the European Union. https://doi.org/10.2760/928418

Tripathy, K. P., Mukherjee, S., Mishra, A. K., Mann, M. E., & Williams, A. P. (2023). Climate change will accelerate the high-end risk of compound drought and heatwave events. *Proceedings of the National Academy of Sciences*, *120*(28), e2219825120. https://doi.org/10.1073/pnas.2219825120

Tuel, A., & Martius, O. (2021). A climatology of sub-seasonal temporal clustering of extreme precipitation in Switzerland and its links to extreme discharge. *Natural Hazards and Earth System Sciences*, *21*(10), 2949–2972. https://doi.org/10.5194/nhess-21-2949-2021

Vitart, F., & Robertson, A. W. (2018). The sub-seasonal to seasonal prediction project (S2S) and the prediction of extreme events. *npj Climate and Atmospheric Science*, *1*(1), 3. https://doi.org/10.1038/s41612-018-0013-0

Vogel, M. M., Orth, R., Cheruy, F., Hagemann, S., Lorenz, R., van den Hurk, B. J., & Seneviratne, S. I. (2017). Regional amplification of projected changes in extreme temperatures strongly controlled by soil moisture-temperature feedbacks. *Geophysical Research Letters*, *44*(3), 1511–1519. https://doi.org/10.1002/2016GL071235

von Luxburg, U. (2007). A tutorial on spectral clustering. *Statistics and Computing*, *17*(4), 395–416. https://doi.org/10.1007/s11222-007-9033-z

Wang, A., Zhang, M., Chen, E., Zhang, C., & Han, Y. (2024). Impact of seasonal global land surface temperature (LST) change on gross primary production (GPP) in the early 21st century. *Sustainable Cities and Society*, *110*, 105572. https://doi.org/10.1016/j.scs.2024.105572

Wang, B., Biasutti, M., Byrne, M. P., Castro, C., Chang, C.-P., Cook, K., et al. (2021). Monsoons climate change assessment. *Bulletin of the American Meteorological Society*, *102*(1), E1–E19. https://doi.org/10.1175/BAMS-D-19-0335.1

Wang, Z., Chen, W., Piao, J., Cai, Q., Chen, S., & Xue, X. (2025). Synergistic effects of high atmospheric and soil dryness on record-breaking decreases in vegetation productivity over Southwest China in 2023. *npj Climate and Atmospheric Science*, *8*(1), 6. https://doi.org/10.1038/s41612-025-00895-3

Weynants, M., Ji, C., Linscheid, N., Weber, U., Mahecha, M. D., & Gans, F. (2025). Dheed: An ERA5 based global database of compound dry and hot extreme events from 1950 to 2023. *Earth System Science Data*, *17*(11), 6621–6645. https://doi.org/10.5194/essd-17-6621-2025

White, C. J., Domeisen, D. I. V., Acharya, N., Adefisan, E. A., Anderson, M. L., Aura, S., et al. (2022). Advances in the application and utility of subseasonal-to-seasonal predictions. *Bulletin of the American Meteorological Society*, *103*(6), E1448–E1472. https://doi.org/10.1175/BAMS-D-20-0224.1

Wu, R., Huang, A., Huang, D., Tang, J., & Xu, X. (2025). Characteristics of the summer regional precipitation events in the middle and lower Yangtze River Basin and associated mechanisms. *Journal of Geophysical Research: Atmospheres*, *130*(3), e2024JD042622. https://doi.org/10.1029/2024JD042622

Wu, H., Su, X., & Singh, V. P. (2023). Increasing risks of future compound climate extremes with warming over global land masses. *Earth's Future*, *11*(9), e2022EF003466. https://doi.org/10.1029/2022EF003466

Wu, X., Hao, Z., Tang, Q., Singh, V. P., Zhang, X., & Hao, F. (2021). Projected increase in compound dry and hot events over global land areas. *International Journal of Climatology*, *41*(1), 393–403. https://doi.org/10.1002/joc.6626

Xiong, H., Han, J., & Yang, Y. (2025). Propagation from meteorological to hydrological drought: Characteristics and influencing factors. *Water Resources Research*, *61*(4), e2024WR037765. https://doi.org/10.1029/2024wr037765

Xu, P., Wang, L., Chen, W., Chen, G., & Kang, I.-S. (2020). Intraseasonal variations of the British–Baikal corridor pattern. *Journal of Climate*, *33*(6), 2183–2200. https://doi.org/10.1175/jcli-d-19-0458.1

Xu, W., Yuan, W., Wu, D., Zhang, Y., Shen, R., Xia, X., et al. (2024). Impacts of record-breaking compound heatwave and drought events in 2022 China on vegetation growth. *Agricultural and Forest Meteorology*, *344*, 109799. https://doi.org/10.1016/j.agrformet.2023.109799

Xu, X., Huang, A., Huang, D., Zhang, Y., Gu, C., Cai, S., et al. (2023). What are the dominant synoptic patterns leading to the summer regional hourly extreme precipitation events over central-eastern Tibetan Plateau and Sichuan Basin? *Geophysical Research Letters*, *50*(5), e2022GL102342. https://doi.org/10.1029/2022GL102342

Yihui, D., & Chan, J. C. (2005). The East Asian summer monsoon: An overview. *Meteorology and Atmospheric Physics*, *89*(1), 117–142. https://doi.org/10.1007/s00703-005-0125-z

Yim, S.-Y., Wang, B., & Kwon, M. (2014). Interdecadal change of the controlling mechanisms for East Asian early summer rainfall variation around the mid-1990s. *Climate Dynamics*, *42*(5), 1325–1333. https://doi.org/10.1007/s00382-013-1760-6

Yin, H., Wu, Z., & He, H. (2025). Interpreting seasonal droughts over the Yangtze River Basin utilizing anomalies of local-scale atmospheric circulation. *Journal of Hydrology: Regional Studies*, *58*, 102231. https://doi.org/10.1016/j.ejrh.2025.102231

Yuan, X., Wang, L., Wu, P., Ji, P., Sheffield, J., & Zhang, M. (2019). Anthropogenic shift towards higher risk of flash drought over China. *Nature Communications*, *10*(1), 4661. https://doi.org/10.1038/s41467-019-12692-7

Yuan, X., Wang, Y., Ji, P., Wu, P., Sheffield, J., & Otkin, J. A. (2023). A global transition to flash droughts under climate change. *Science*, *380*(6641), 187–191. https://doi.org/10.1126/science.abn6301

Yuan, X., Wang, Y., Zhou, S., & Li, H. (2024). Multiscale causes of the 2022 Yangtze mega-flash drought under climate change. *Science China Earth Sciences*, *67*(8), 2649–2660. https://doi.org/10.1007/s11430-024-1356-x

Yue, S., & Wang, C. (2004). The Mann-Kendall test modified by effective sample size to detect trend in serially correlated hydrological series. *Water Resources Management*, *18*(3), 201–218. https://doi.org/10.1023/B:WARM.0000043140.61082.60

Zeng, J., Xue, D., & Huang, D. (2025). Comparison for the characteristics and mechanisms of independent daytime, nighttime, and compound heatwaves over Yangtze-Huaihe River Basin. *Journal of Geophysical Research: Atmospheres*, *130*(7), e2024JD042683. https://doi.org/10.1029/2024JD042683

Zhang, L., & Zhou, T. (2015). Drought over East Asia: A review. *Journal of Climate*, *28*(8), 3375–3399. https://doi.org/10.1175/JCLI-D-14-00259.1

Zhang, X., Zhou, T., Zhang, W., Ren, L., Jiang, J., Hu, S., et al. (2023). Increased impact of heat domes on 2021-like heat extremes in North America under global warming. *Nature Communications*, *14*(1), 1690. https://doi.org/10.1038/s41467-023-37309-y

Zhang, Y., Liu, X.-M., Wang, K.-W., Bai, P., Li, X. Y., Jiang, H. N., et al. (2026). Hydrologic responses to hot droughts in the Yangtze River Basin. *Advances in Climate Change Research*, *17*(2), 400–410. https://doi.org/10.1016/j.accre.2025.12.005

Zhou, C., Wang, G., Jiang, H., Li, S., Shi, X., Hu, Y., & Cabral, P. (2025). Spatio-temporal patterns of compound dry-hot extremes in China. *Atmospheric Research*, *314*, 107795. https://doi.org/10.1016/j.atmosres.2024.107795

Zscheischler, J., Martius, O., Westra, S., Bevacqua, E., Raymond, C., Horton, R. M., et al. (2020). A typology of compound weather and climate events. *Nature Reviews Earth & Environment*, *1*(7), 333–347. https://doi.org/10.1038/s43017-020-0060-z

Zscheischler, J., Westra, S., Van Den Hurk, B. J., Seneviratne, S. I., Ward, P. J., Pitman, A., et al. (2018). Future climate risk from compound events. *Nature Climate Change*, *8*(6), 469–477. https://doi.org/10.1038/s41558-018-0156-3